UNIVERSITÀ DEGLI STUDI DI PADOVA

DIPARTIMENTO DI INGEGNERIA INDUSTRIALE

CORSO DI LAUREA MAGISTRALE IN INGEGNERIA CHIMICA E DEI PROCESSI INDUSTRIALI

Tesi di Laurea Magistrale in
Ingegneria Chimica e dei Processi Industriali

Development of on-chip mixing and incubation platform for the loading of extracellular vesicles with an anti-cancer drug

Relatore: Prof.ssa Elisa Cimetta
Correlatore: Dott.ssa Caterina Piunti

Laureando: FRANCESCO DE NICOLO

ANNO ACCADEMICO 2021 – 2022

Riassunto

Nonostante i notevoli progressi raggiunti nello studio del cancro, le metastasi sono ancora sinonimo di malattia terminale. Pertanto, lo sviluppo di terapie mirate è un imperativo clinico.

Negli ultimi anni, si è scoperto che le vescicole extracellulari (EVs) sono coinvolte nella progressione di numerosi tumori. Le EVs sono vescicole di dimensioni nanometriche rilasciate da diversi tipi di cellule sia in condizioni normali che patologiche, le quali trasportano informazioni favorendo alcuni importanti processi come l'angiogenesi, le metastasi, la resistenza ai farmaci e la proliferazione del cancro. Ad esempio, si è scoperto che le EVs derivate dal Neuroblastoma (NB) - uno dei più comuni tumori solidi dell'infanzia - hanno un ruolo nella sua progressione metastatica.

Dal punto di vista terapeutico, le EVs rappresentano un eccellente sistema di somministrazione di farmaci: sono dotate, infatti, di numerose proprietà intrinseche, quali una lunga emivita, un'ottima tolleranza da parte dell'organismo e la capacità di essere internalizzate da cellule riceventi.

Sebbene le EVs abbiano mostrato promettenti applicazioni terapeutiche, sono ancora necessari ampi sforzi multidisciplinari.

Le microfluidica potrebbe essere uno strumento prezioso per l'ingegnerizzazione delle EVs: le odierne tecnologie di microscala permettono di condurre esperimenti più complessi, con maggior controllo e precisione, divenendo una modalità di ricerca sempre più affermata, soprattutto in campo biomedico.

Considerando queste premesse, l'obiettivo del lavoro di tesi è la progettazione e lo sviluppo di un dispositivo microfluidico per la generazione di EVs caricate con farmaci. Le EVs, una volta isolate da cellule staminali mesenchimali (MSCs), possono essere ingegnerizzate con vari agenti terapeutici, tra cui la Verteporfina (VP). La VP è una piccola porfirina idrofobica che ha recentemente fornito risultati positivi per la sua attività antitumorale in diversi tipi di cancro, tra cui il NB.

La piattaforma è stata progettata utilizzando AutoCAD® in modo da ottenere una perfetta miscelazione tra le EVs e la VP all'interno dell'unità di miscelazione e un perfetto tempo di incubazione. La piattaforma è stata quindi modellata, eseguendo simulazioni di fluidodinamica computazionale con COMSOL Multiphysics®. Lo stampo è stato fabbricato con la tecnica di fotolitografia e le repliche in polidimetilsilossano (PDMS) dei chip sono state ottenute mediante replica molding. Il trattamento al plasma viene utilizzato per conferire una tenuta idraulica irreversibile della piattaforma microfluidica su un supporto di vetro. Il chip microfluidico in questa configurazione viene utilizzato per eseguire validazioni

fluidodinamiche e biologiche. Infine, sono stati condotti esperimenti preliminari per studiare l'effetto delle EVs caricate con VP su cellule bersaglio di NB.
Una volta che la tecnologia sarà messa a punto, avrà il potenziale per far progredire lo sviluppo di terapie innovative, sfruttando le EVs come vettori adatti alla consegna di farmaci.

Summary

Despite great progress achieved in the understanding of cancer biology, metastases are still synonymous of terminal illness. Therefore, developing targeted therapies for cancer is a clinical imperative.

In recent years, extracellular vesicles (EVs) have been found to be involved in cancer development. EVs are nano-sized vesicles released from different cell types under both normal and pathological conditions that carry information leading to some important processes such as angiogenesis, metastasis, drug resistance and proliferation in cancer. For instance, EVs derived from Neuroblastoma (NB) - one of the most common solid tumors of childhood - are found to play a role in mediating its progression.
From a therapeutic point of view, EVs represent an excellent drug delivery system: EVs intrinsically possess many attributes of drug delivery systems, since these particles have a long-circulating half-life, are well tolerated in the body, and are internalized by recipient cells.

Although EVs have displayed some promising therapeutic applications, extensive multi-disciplinary efforts are still needed.

Microfluidic technologies could be a valuable tool for the engineering of EVs, owing to the low amount of reagents and samples needed, high throughput and different phenomena that characterize this technology with respect to their large-scale counterparts.

Considering such promises, the aim of the project is the design and development of a microfluidic device for generating drug-loaded EVs using microfluidic mixing and incubation. Mesenchymal Stem Cells (MSCs) are used as cell sources of EVs. EVs can be loaded with various therapeutic agents, including Verteporfin (VP). VP is a small hydrophobic porphyrin that recently provided positive results for its anti-cancer activity in different tumors, including NB.

The platform is designed using AutoCAD® so that both a perfect mixing between MSCs-derived EVs and VP occurs within the mixing unit and the desired incubation time is achieved. The platform is then modeled, performing computational fluid dynamics simulations through COMSOL Multiphysics®. The master mold is fabricated with photolithography, and polydimethylsiloxane (PDMS) replicas of the chips were obtained with replica molding processes. Plasma treatment is used to form an irreversible hydraulic seal of the microfluidic platform to a glass support. The platform in this configuration is used to perform both fluid dynamic and biological validations. Finally, preliminary experiments are carried out to study the effect of VP-loaded EVs on NB target cells. Although the utilization of EVs for therapeutic drug delivery is still in its infancy, a more

advanced understanding and systemic evaluation of their use will boost the development of EVs as a superior and effective drug delivery system that can bring breakthroughs to the field of cancer nanomedicine.

Table of Contents

List of Figure

List of Tables

Introduction

Microfluidics, the discipline that studies fluids at the nanoscale and micro liter scale, enables miniaturization of laboratory operations by realizing what are commonly referred to as lab-on-a-chip.

Microscale technologies have many advantages, such as handling small volumes, improving process automation, and reducing experimental time. All these features make microfluidics an excellent candidate for applications in various scientific fields, including biomedicine.

In recent years, it was discovered that extracellular vesicles (EVs)-small vesicles released from different cell types-are involved in cancer development. For example, EVs derived from neuroblastoma (NB)-one of the most common pediatric cancers-have been found to play a role in mediating metastasis.

Despite being responsible for cancer progression, EVs could also potentially play a role in cancer treatment by turning them into drug delivery systems.

The laboratory in which this thesis work is carried out - the BIAMET (Biomedical Applications of Multiscale Engineering Technologies) Lab - is a place where engineers and biologists work together with the primary objective of studying the role of EVs in NB.

The goal of this thesis is to design and develop a microfluidic platform capable of generating drug-loaded EVs to facilitate targeted drug delivery in NB.

The first Chapter presents a general overview of microfluidics and its role in the field of biomedical research. The focus is on specific microfluidic devices, their materials and technologies, manufacturing techniques, and the benefits associated with their use. The chapter also includes a brief description of NB and the role of EVs both in tumor progression and as drug delivery systems.

The second Chapter discusses the platform designs and conditions implemented in COMSOL Multiphysics® for fluid dynamic simulations. The materials and procedures for master and platform production, as well as fluid dynamic and biological validations are then described. Finally, protocols and biological experiments to evaluate the presence of VPs in EVs are presented.

In the last Chapter, the rationale for modifying the platform geometry is first discussed. Next, the results of COMSOL Multiphysics® *steady-state* and *time-dependent* simulations are compared with those provided by fluid dynamic validations to confirm the expected behavior of the platforms. In addition, some considerations on biological validation and experiment results are reported. In particular, pre-treatment and post-treatment characterizations are shown, as well as the comparison between *off-chip* and *on-chip* protocols to evaluate the difference in loading efficiency. Finally, preliminary immunofluorescence and MTT assay

results are performed to verify the potential therapeutic effects of VP-loaded EVs on NB target cells.

In the Conclusions, a brief overview of this thesis is provided, focusing on the results obtained and suggestions for future work.

Chapter 1

State of the Art

In this chapter an overview of microfluidics, its basic concepts, the physical phenomena that govern the micro-scale, and the main applications, especially in the biomedical field, are illustrated. Then, a brief description of Neuroblastoma and the role of extracellular vesicles both in cellular communication and as drug delivery systems is presented. Finally, the aim of the project is reported.

1.1 Microfluidics

Microfluidics is a discipline that studies fluid behavior in miniaturized systems, taking origins from the micro-electromechanical systems, the so-called MEMS, which had the initial deal to use smaller quantities of reagents. Haeberle & Zengerle (2007) support that the first applications are dated back to 1979, a milestone year for microfluidics, and concern analytical techniques, such as gas chromatography (GC) or high-pressure liquid chromatography (HPLC). Over the past two decades, microfluidics technologies have become more and more complex platforms in which some unit operations like valves, mixers, and pumps are implemented for better control of the fluid.
The handling of small volumes is not the only benefit of microfluidics; according to Dittrich & Manz (2006) microfluidic chips guarantee to process fluids in a continuous and parallel way, resulting in:

- Better automation;
- Possible achievement of steady-state condition;
- Higher throughput;
- Higher efficiency;
- Shorter experimental time;
- Reduction of the total cost of experiments.

Moreover, it is noteworthy that at the micro-scale the dominant physics phenomena are different from the macro-scale, resulting in a more controllable process. In microfluidic systems, the increase of the surface-to-volume ratio and the short distances lead to a faster and more tunable mass and heat transport. Squires & Quake (2005) explain how these micro-scale phenomena are exploited in different applications such as protein crystallization, clinical and forensic analysis, micropumps, and proteomics, rather than molecular

diagnostic, fuel cells, and separation operations. Thus, it is evident that the high multidisciplinary of microfluidics makes it an interesting science for many fields such as chemistry, medicine, pharmaceuticals, biology, health, and energy generation.

1.1.1 Physics of microfluidics

As anticipated in §1.1, the governing phenomena at the micro-scale are different from those of the macro-scale: the small dimensions imply a change in transport phenomena. Dimensionless numbers, summarized in Table 1.1, are used in microfluidics to compare phenomena or length scales playing a fundamental role in the comprehension of the dominant forces and the behavior of fluids.

Table 1.3 *Dimensionless numbers used in microfluidics (Squires & Quake, 2005).*

Acronym	Name	Phenomena compared
Re	Reynolds	Inertial/viscous
Pe	Péclet	Convection/diffusion
Ca	Capillary	Viscous/interfacial
Wi	Weissenberg	Polymer relaxation time/shear
De	Deborah	Polymer relaxation time/flow
El	Elasticity	Elastic effects/inertial effects
Gr	Graschof	Re for buoyant flow
Ra	Rayleigh	Pe for buoyant flow
Kn	Knudsen	Slip length/macroscopic length

Before introducing the most used dimensionless numbers (Re, Pe, Ca), some meaningful equations, related to transport phenomena, are recalled. The motion of a Newtonian fluid is described by the Navier-Stokes equation, reported in 1.1:

$$\rho \frac{D\,(\boldsymbol{v})}{Dt} = \rho\left(\frac{\partial \boldsymbol{v}}{\partial t} + (\boldsymbol{v}\cdot\nabla)\boldsymbol{v}\right) = \mu\nabla^2(\boldsymbol{v}) - \nabla P + \rho g \quad (1.1)$$

Where the term on the right, composed respectively by the sum of the velocity variation along the time and the convective term, represents the substantial derivative of the velocity vector $\boldsymbol{v}$ [m/s], while on the left, the diffusion term, the pressure [Pa], and gravity forces [m/s^2] can be denoted.

As described by Squires & Quake (2005), in microfluidic systems the viscous forces predominate over the inertial ones, and consequently, the convective term $(\boldsymbol{v}\cdot\nabla)\boldsymbol{v}$ can be neglected.

The comparison between inertial and viscous forces is defined as Reynolds number (Re) and allows the distinction of the regime into laminar or turbulent:

$$Re \equiv \frac{\rho v D}{\mu} \tag{1.2}$$

Where ρ is the fluid density, usually expressed in [kg/m^3], v is the characteristic velocity of fluid [m/s], μ is the fluid viscosity [Pa·s], and D is the pipe diameter. If the pipe is not tubular, the diameter is calculated as an equivalent diameter through Equation 1.3:

$$D_{eq} \equiv \frac{4S}{2P} \tag{1.3}$$

Where S is the area available for the passage of the fluid [m^2] and P is the semi-perimeter [m]. Beebe *et al.* (2002) reported that in a tubular pipe, for Re < 2300 the fluid is in a laminar regime while for Re>2300 the flow is turbulent, thus characterized by the presence of eddies leading to instability and unpredictability. As expressed in Breslauer *et al.* (2006), generally, in microfluidic systems, thanks to the small dimensions, the fluid behaves in a laminar way which is highly predictable and allows to simplify the Navier-Stokes and the mass transport balance equations. Under this assumption, Equation 1.1 can be easily solved, obtaining the Hagen Poiseuille equation:

$$v = 2V\left(1 - \frac{r^2}{R^2}\right) \tag{1.4}$$

Where V is the ratio between the volumetric flow rate and the cross-sectional area [m/s], whereas R is the radius of pipe [m]. The result is shown in Figure 1.1: the velocity profile has a parabolic behavior with its maximum value $v_{max} = 2\text{V}$ in $r = 0$, while $v = 0$ at the wall $r = R$.

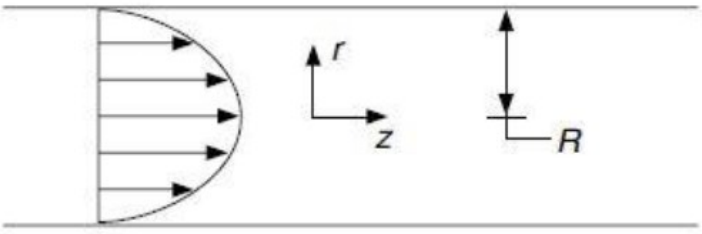

Figure 19.1 *Velocity profile for a laminar flow in a pipe (*Perry's Chemical Engineers' Handbook*, 2008).*

Another significant dimensionless number is the Péclet number (Pe) which compares the phenomena of convection and diffusion concerning mass transport. The definition is expressed in Equation 1.5:

$$Pe \equiv \frac{vD}{D_i} \tag{1.5}$$

Where v is the velocity inside the pipe [m/s], D is the pipe diameter [m], and D_i is the diffusion coefficient of the species i [m^2/s]. The coefficient D_i can be computed thanks to the Einstein-Smoluchowski equation:

$$D_i = \eta k_B T \tag{1.6}$$

Where η is the mobility of the particles [kg/s], k_B is the Boltzmann constant [J/K], and T is the temperature [K]. Under the assumption of movement of spherical particles in a viscous fluid, the Einstein-Smoluchowski equation becomes the Stokes-Einstein equation:

$$D_i = \frac{k_B T}{6\pi\mu r} \tag{1.7}$$

Where r is the radius of the particles [m].
Therefore, a small value of Pe, typically between 0.05 and 500, corresponds to a high contribution of the diffusion term, whereas for a high value of Pe, around 10^3, the dominant transport mechanism is convection.
In microfluidic systems, the absence of eddies, due to the laminar flow, implies a mass transport mainly based on the diffusion mechanism, also resulting in low mixing.
Considering now the conservation equation of species i:

$$\frac{dC_i}{dt} = -\nabla(C_i v) - \nabla(J_i) + R_i \tag{1.8}$$

Where on the left side is the variation of concentration of i along time, and on the right side are the convective and the diffusion fluxes respectively, and the reaction term.
The diffusive flux [mol/m^2s] can be expressed through the Fick law:

$$J_i = -D_i \nabla(C_i) \tag{1.9}$$

In microfluidic devices, as previously described, the convection term is negligible with respect to the diffusion one. Moreover, assuming that a steady state is achieved and no reaction takes place, Equation 1.8 can be simplified:

$$0 = D_{m,i} \nabla^2(C_i) \tag{1.10}$$

In conclusion, the last relevant dimensionless number is the Capillary number (Ca) defined as:

$$Ca = \frac{\mu v}{\gamma} \tag{1.11}$$

Where μ is the fluid viscosity [Pa·s], v is the velocity inside the channel [m/s], and γ is the surface tension of the fluid [N/m], usually with air. Ca relates the viscous forces with the surface tension and play an important role in immiscible fluids: in this case, as explained by Squires & Quake (2005), surface tension affects the dynamics of the free surface.

1.1.2 Micromixing

As stated previously, increasingly complex microfluidic platforms with numerous unit operations have been recently developed. Here, the attention is focused on microfluidic mixing. As described by Fu *et al.* (2006), due to the low Reynolds number characteristic of the micro-scale, mixing is driven principally by laminar flow and diffusion, and consequently a long time is required to reach homogeneity. To design a more effective mixing system, and favor the diffusion rate, it is necessary to minimize the thickness and increase the contact surface between the fluids. Chaotic advection and turbulence may also contribute: Lee *et al.* (2016) support that their generation introduces irregularity in fluid movement, producing a random variation in space and time of pressure and velocity.
Two other valuable parameters in addition to the Re and Pe numbers can be evaluated to quantify the degree of mixing enhancement: the mixing index and the mixing performance. The mixing index η is defined by Sarkar *et al.* (2014) as:

$$\eta = 1 - \sqrt{\frac{\gamma^2}{\gamma_{max}^2}} \tag{1.12}$$

Where γ^2 is the variance calculated at the desired cross-sectional area, whereas γ_{max}^2 is the maximum variance. The variance is defined in Equation 1.13:

$$\gamma^2 = \frac{1}{n}\sum_{i=1}^{n}(c_i - \bar{c}) \tag{1.13}$$

Where n is the number of sampling points, c_i is the concentration of solute at the sampling point and $\bar{c}$ is the average concentration of solute. Note that the values of mixing index η are 0 for entirely unmixed fluids and 1 for completely mixed fluids.
The mixing performance (MP) considers the effect of pressure drops through the mixer. The definition reported by Sarkar *et al.* (2014) is:

$$MP = \frac{\eta}{\Delta P^*} \tag{1.14}$$

Where η is the mixing index and ΔP^* is the dimensionless pressure drop, expressed as:

$$\Delta P^* = \frac{\Delta P}{\rho v^2} = \frac{P_{in} - P_{out}}{\rho v^2} \tag{1.15}$$

Where ΔP is the difference between the inlet and the outlet pressure, ρ is the fluid density, and v is the average velocity.

To improve contribution phenomena, *i.e.* chaotic advection and diffusion, several strategies exist; the most employed are active and passive micromixers.

According to Tripathi *et al.* (2021), active micromixers require the intervention of external energy sources, such as acoustic field, electrokinetics, magnetic field, and thermal energy, capable to promote fluid disturbances. Even though active methods produce a greater effect than passive ones, the high energy consumption, and high costs in device integration slow down their applicability.

On the other hand, passive micromixers represent the easiest method, since only pumping energy is needed. As claimed by Lee *et al.* (2016), the basic idea is to modify the channel shape either for stretching, splitting, folding, and breaking the flow, all actions that increase the chaotic advection; or feeding the samples through holes, cantilever plate valves or multi-channel, to obtain a growth in the molecular diffusion. Following these criteria, passive micromixers can be distinguished in lamination-based and chaotic advection-based. The lamination-based micromixers are equipped with either "T" or "Y" inlet shape. The chaotic advection-based micromixers, illustrated in Figure 1.2, can be classified in different categories, depending on their structure:

- Intersecting channels;
- Convergent-divergent channels;
- Three-dimensional structures;
- Embedded barriers;
- Staggered herringbone structures;
- Twisted channels.

Specifically, the embedded barriers represent the simplest chaotic advection-based micromixers, created by the addition of obstacles in the fluid pathway.

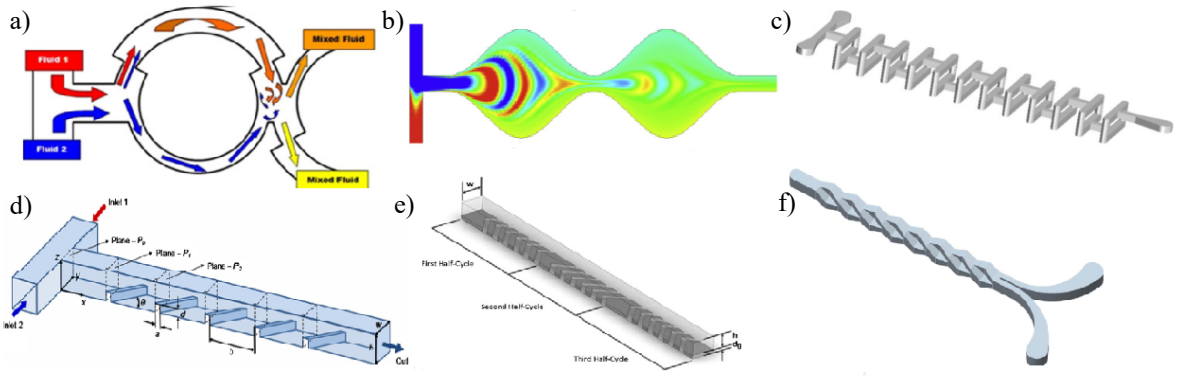

Figure 1.20 *Different models of chaotic advection-based micromixers: intersecting channels (a), convergent-divergent channels (b), three-dimensional structures (c), embedded barriers (d), staggered herringbone structures (e), twisted channels (f) (Lee et al., 2016).*

An example is provided by Fang *et al.* (2012) in which a micromixer characterized by a T-type inlet and a mixing unit with staggered bars, that disturb the flow field, is developed. The computer simulation, represented in Figure 1.3, results in a rise in the mixing performances if the number of mixing units increases.

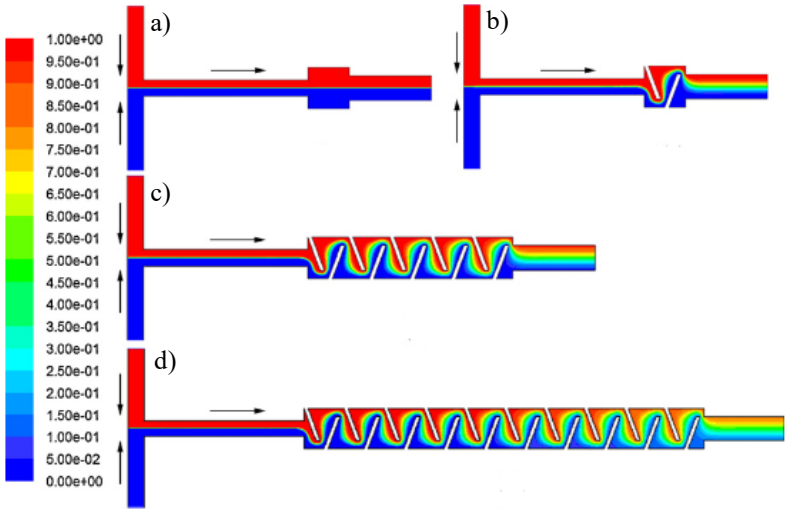

Figure 1.21 *Mass fraction contour plot of the T channel with (a) 0, (b) 1, (c) 5, (d) 10 embedded barrier mixing units at a flow rate of 20 µL/s. The arrows indicate the flow direction (Fang et al., 2012).*

Another example is the study conducted by Yuan *et al.* (2022), in which many baffle configurations are investigated, as illustrated in Figure 1.4.

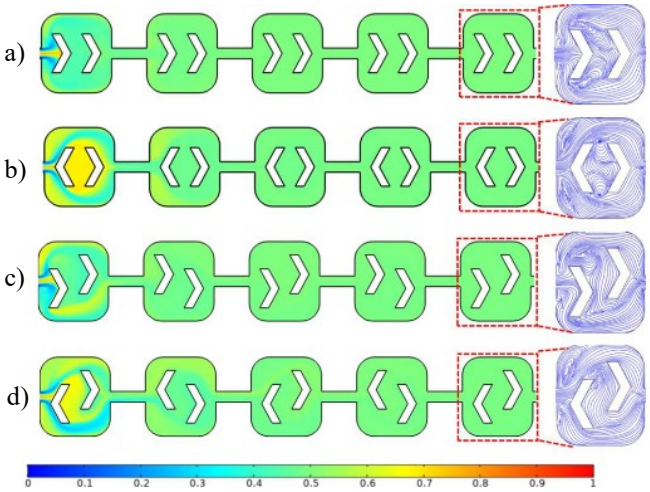

Figure 1.22 *The distributions of concentration and streamline of symmetrical configurations (a) and (b), and asymmetrical configurations (c) and (d) (Yuan et al., 2022).*

The analysis shows the achievement of a better homogeneity at Re lower than 1 in symmetrical configurations (Figures 1.4 (a) and (b)), since the mixing is principally driven by diffusion; at higher Re an intensification of chaotic advection appears, causing improved mixing in asymmetrical configurations (Figure 1.4 (c) and (d)).

The value of Re also affects pressure loss: Figure 1.5, indeed, shows that at low Re there is no significant difference in pressure drop among the investigated configurations, which is noticeable when Re increases.

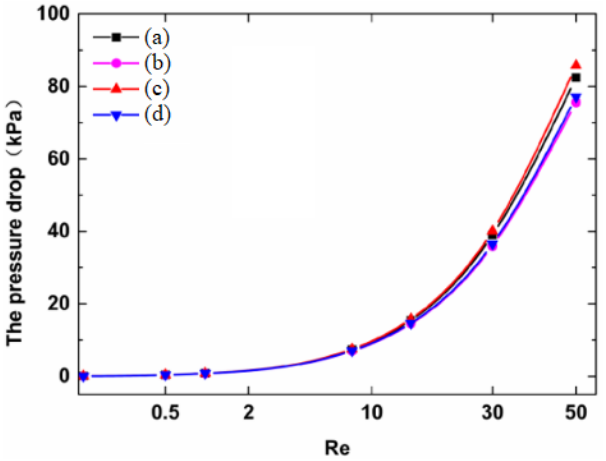

Figure 1.23 *Pressure drops as a function of Re for configurations (a), (b), (c), and (d) (Yuan et al., 2022).*

In conclusion, the study reveals that configurations *b)* and *d)* perform better than *c)* and *d)*.

1.1.3 On-chip incubation

Together with mixing processes, incubation represents another essential operation employed for precise time control in chemical and biochemical reactions. In microfluidics, this module can be integrated with designing platforms consisting of delay-lines, that allow incubation of particles/molecules for exact time periods. Ideally, a proper on-chip incubation device should be characterized by low back pressure, low dispersion of incubation time, and enough flexibility to work in a range of incubation times.

In a study conducted by Frenz *et al.* (2009), a microfluidic system has been developed, shown in Figure 1.5 (a), using two design equations. The first one, reported in Equation 1.16, relates the delay time ϑ to volumetric flowrate and l, w and h, respectively the length, the width, and the height of the delay-line geometry:

$$\vartheta = \frac{lwh}{\dot{V}} \tag{1.16}$$

The second design equation concern the pressure drop estimation, reported in Equation 1.17:

$$P = c\eta \frac{l}{wh^3}\dot{V} \tag{1.17}$$

Where η is the fluid viscosity, $\dot{V}$ is the flowrate used, l, w, and h are the geometric dimensions and c is a constant that depends on the ratio w/h and is defined as:

$$c = 12\left[1 - \frac{192}{\pi^5}\frac{h}{w}tanh\left(\frac{\pi w}{2h}\right)\right]^{-1} \tag{1.18}$$

As reported in the article, pressure drop represents one of the two problems in incubation design. From Equation 1.17 it is evident that pressure drop is mainly affected by the height of the channel owing to the inverse cube dependence: thus, an increase in height leads to a decrease in pressure drop.

The other problem associated with on-chip incubation is the so-called dispersion of incubation times. The well-known Hagen Poiseuille flow characterized by a parabolic velocity profile, causes diversity in particle rates between the center and the walls, producing significant differences in terms of incubation time. To address this issue, named Taylor dispersion, Frenz *et al.* (2009) have inserted some constrictions, observable in Figure 1.6 (b), capable to re-mix the flow that permits the reduction in time dispersion.

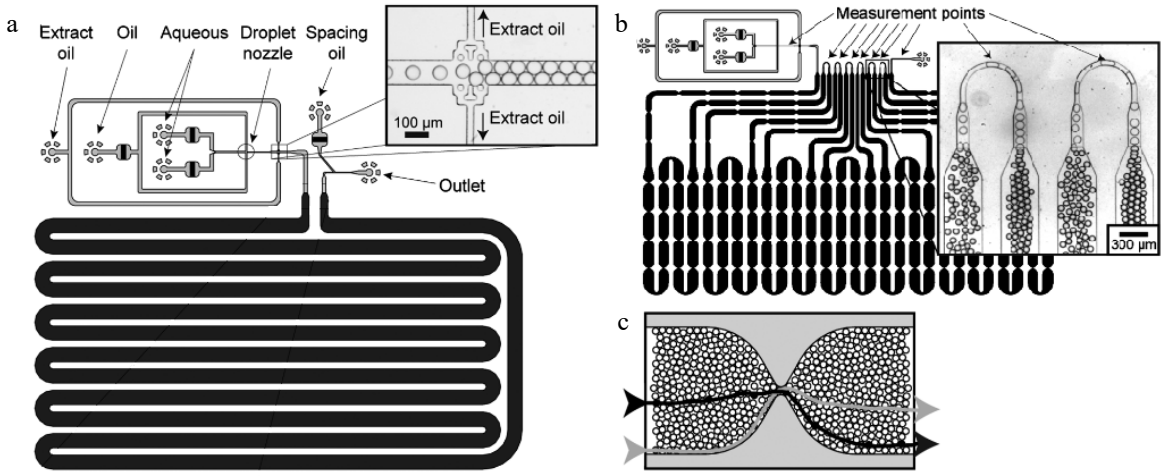

Figure 1.24 *On-chip incubation: (a) microfluidic platforms with delay-lines to control the incubation time of single particles; (b) microfluidic platforms for on-on chip incubation with constriction to avoid the Taylor dispersion phenomenon; (c) redistribution of the particles due to the constriction (Frenz et al., 2009).*

1.1.4 Microfluidics in Biology

As mentioned earlier, microfluidics has a high versatility that enables its application in many fields, including biological applications. One of the most important aims of the biological field is the complete understanding of the cellular mechanisms, by studying the intra- and inter-cellular interactions that contribute to trigger and coordinate cellular events.
Standard *in vitro* techniques are not able to represent in a comprehensive way the complex *in vivo* milieu that characterizes the cellular environment, lacking a precise control of culture conditions and being limited by the large volumes needed. (Gao *et al.*, 2012).
Compared to their large-scale counterparts, microfluidics offers the possibility to overcome some issues, resulting in a valuable tool for biological studies thanks to:

- Small volumes of reagents and waste produced that lead also to a reduction in the operating costs;
- Precise control of cell numbers in a given volume. For instance, through a droplet generation system, guaranteeing the manipulation of individual cells for single-cell investigation;
- Possibility to arrange cells in specific positions to obtain high-precision perturbation experiments;
- The laminar flow that enables the creation of concentration gradient controllable in space and time;
- Achievement of the stationary condition, if the platform works continuously;
- Device reliability and high throughput experiments;
- Possibility of using optically transparent materials that allow live observation with the microscope.

Although huge progress has been made in microfluidics, some limitations still represent a challenge. For instance:

- Faster consumption of nutrients and an increase in the concentration of metabolites due to small volumes;
- Lack of standardized and published cellular protocols for microfluidics due to the novelty of the field.

Despite these drawbacks, microfluidic technology has shown unique capabilities for triggering the fast growth of biomedical research.

1.2 Microfluidic devices: materials and technologies

So far, the physics of microfluidics and their applications have been the core of the study: laminar flow and short distances represent the main features of these devices. In the following sections, the focus is shifted to both the technique and the material involved in the fabrication of microfluidic devices. As mentioned in the review of Niculescu *et al.* (2021) each material has different properties and different behavior when it is processed, meaning that the proper method of production must be chosen and adapted. Generally, the manufacturing process distinguishes two steps, that will be described in detail below: firstly, the design and production of the master and then the realization of the platform.

1.2.1 Design and production of the master

The master is usually designed using a 2D and 3D environment of the AutoCAD® software. Afterwards, a fluid dynamic simulation of the designed geometry is performed with the help of COMSOL Multiphysics® modelling software. At this point, the master can be produced through a mechanical process, the most important being photo- and soft lithography.

1.2.1.1 Photolithography

Photolithography is a patterning technique that allows the creation of a mold, also called master mold, to reproduce micrometric structures, as claimed by Weibel *et al.* (2007). It is a cheap and fast technique, characterized by a resolution from a few microns to hundreds of nanometers.

Figure 1.7 shows an overview of the process of master fabrication. Briefly, a silicon wafer is cleaned and dried (Figure 1.7a) to allow the deposition of a photosensitive resin with a specific thickness (Figure 1.7b). At this point, a photomask, a sheet of a transparent polymer with the desired design printed, is placed on the layer of photoresist (Figure 1.7c). Then, the

support is exposed to UV light that selectively polymerizes the resin. Finally, after removing the mask and the unpolymerized residues, a rigid master is obtained.

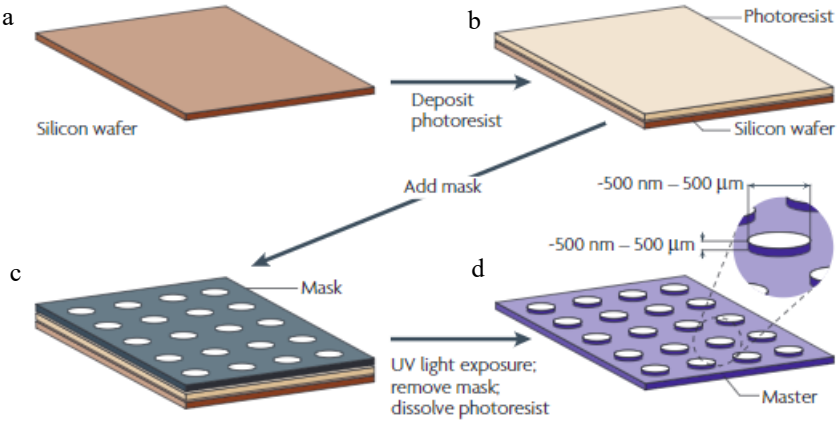

Figure 1.25 *Fabrication of the rigid master with photo lithography: (a) silicon wafer; (b) deposition of the photoresist on the silicon wafer; (c) deposition of the mask; (d) exposure to UV light and removal of the mask (Weibel et al., 2007).*

1.2.2 Production of the platform

As previously mentioned, microfluidic platforms are produced through several methods. Among the most important, replica molding is examined, whereby the device can be replicated from an existing master using a polymer.

1.2.2.1 PDMS

Niculescu *et al.* (2021) argue that the choice of material is an extremely important step in microfluidic chip manufacturing since it must guarantee durability, ease of fabrication, transparency, biocompatibility, chemical compatibility, stability at temperature and pressure operating conditions. Initially, silicon and glass are the most commonly employed materials for the fabrication of microfluidic devices. Since neither silicon nor glass match all the required properties for biology and biomedical fields, they have been replaced by polymers, less expensive and characterized by low-cost manufacturing techniques. Among the variety of this category, poly-(dimethylsiloxane) (PDMS) represents an optimal material because of its cheapness and ease of use. From a chemical point of view, PDMS is a linear polymer of silicon origin composed of the repetition of the dimethylsiloxane monomer, as shown in Figure 1.8.

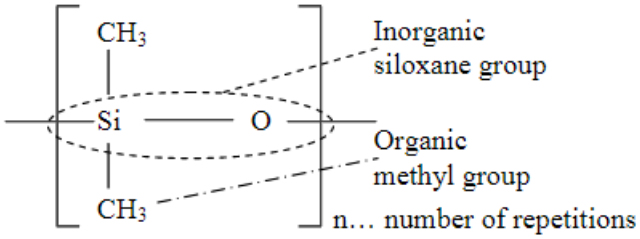

Figure 1.26 *Poly-(dimethylsiloxane) structure (Kuncová-Kallio & Kallio, 2006).*

Together with the aforementioned properties, other characteristics are reported by Weibel *et al.* (2007):

- Biocompatibility;
- Non-cytotoxicity;
- Autoclavable;
- Chemical and thermal stability;
- Optical transparency, allowing microscopic analysis;
- Natural hydrophobicity;
- High elasticity;
- Gas permeability towards O_2, CO_2, and N_2.

Nevertheless, the same advantages can create obstacles, as reported in Kim *et al.* (2007):

- Porosity typical of PDMS can cause the absorption of hydrophobic molecules;
- Gas permeability can result in evaporation and changes in osmolality, detrimental to cell cultures.

1.2.2.2 Replica molding

Using replica molding process, a master is used to produce more microfluidic devices. A polymer, usually PDMS, is deposited on the master and cured at high temperatures to induce reticulation. The cured PDMS is then peeled to separate it from the master.

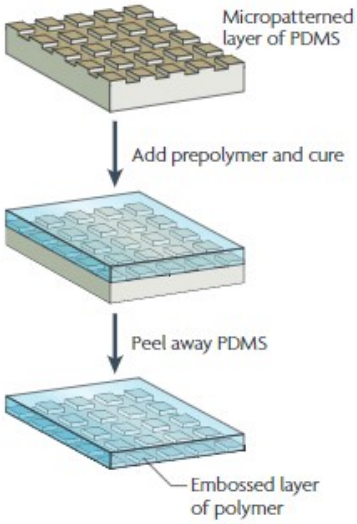

Figure 1.27 *Key stages of replica molding (Weibel et al., 2007).*

1.2.2.3 Plasma treatment

Once the fabrication is completed, the PDMS platform must be sealed to a glass slide obtaining a perfect hydraulic seal. One possibility, and the most convenient, is plasma treatment.

Plasma is the fourth state of matter and is made of partially ionized gas consisting of electrons, ions, and neutral atoms or molecules. Plasma is created at either atmospheric pressure or low pressure in a vacuum chamber, exploiting the generation of an electric field. At sufficiently low pressure, the radio frequency oscillating electric field and the elastic scattering of electrons are combined. Their syllogistic effect leads to the heat of the electrons, which, once achieved an excess in kinetic energy, collide with neutrals and ionization occurs. Choosing the appropriate configuration and operating condition, plasma can be used to clean, activate, etch, or coat the surface. For instance, as discussed by Zhou *et al.* (2010), gases such as nitrogen, oxygen, and hydrogen dissociate and react with the substrate surface creating chemical functional groups.

During the process, illustrated in Figure 1.10, the PDMS and the glass are activated by the plasma, forming on the surface electron-free silicon atoms, and then the silanol groups (Si-O-H), so that some hydrophilicity character appears on the surface.
Subsequently, the two materials, polymer and glass, are brought in contact and covalent bonds Si-O-Si are established.

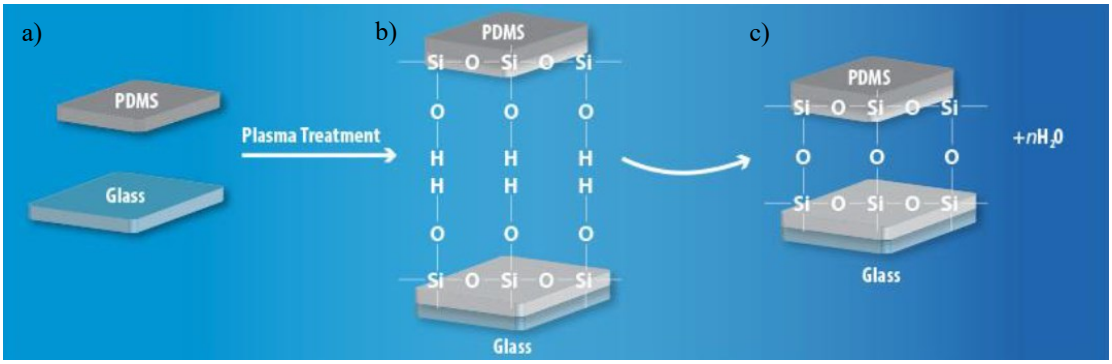

Figure 1.28 *Plasma treatment: (a) single elements of PDMS and glass; (b) activation of the surface; (c) bond creation (https://princetonscientific.com/).*

Plasma treatment shows several advantages:

- Affects only surface properties, without altering the bulk material;
- Forms at near-ambient temperature minimizing the risk of damage to material sensitive to the heat;
- Can be applied to a wide range of materials.

For biological applications, plasma treatment must be performed prior to seeding the cells into the platforms to prevent cellular damage.

1.3 Neuroblastoma

Neuroblastoma (NB) is a rare embryonal solid tumor of the autonomic nervous system and represents one of the most common pediatric diseases, as reported in Davidoff *et al.* (2012). The embryonal origin suggests NB derives from immature nerve-forming cells present in the neural crest tissues, the neuroblasts. Since they are spread throughout the human body, the extracranial tumor can arise in different regions mainly at the sympathetic system level, which regulates essential operations such as breathing and digestion. For instance, as explained by Maris (2010) some affected areas are the neck, upper chest, abdominal, and

pelvis. Figure 1.11 shows some typical pathologies triggered by NB as Horner's syndrome and paralysis due to spinal cord compression.

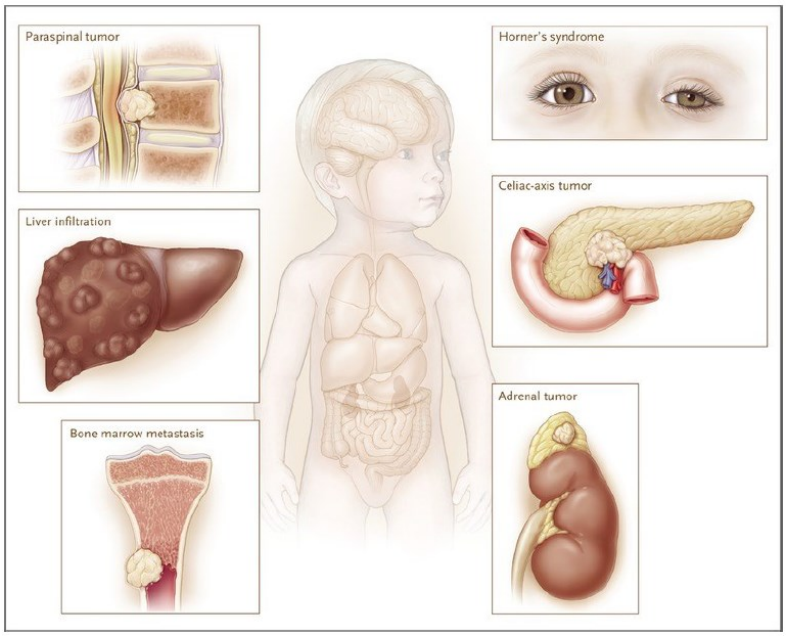

Figure 1.29 *Clinical presentation of NB (Maris, 2010).*

However, the aggressiveness of NB is given also by its metastatic power: tumors diagnosed after the first year of life present problems not only in a localized zone, but also in the abdomen, respiratory system, lymph nodes, and bone marrow. NB cells can also infiltrate organs and surround nerves and vessels, such as the celiac axis, making their mass inaccessible for removal.

According to the severity of the diagnosed cancer, a wide variety of therapy strategies can be applied. As reported in Davidoff *et al.* (2012), for low-risk (LR) patients a resection is usually enough, whereas for intermediate and high-risk (HR) patients a combination of surgery, chemotherapy, radiotherapy, and immunotherapy is recommended. Schramm *et al.* (2015) reported that the International Neuroblastoma Risk Group classified half of all NB as high-risk, characterized by a survival rate of less than 50%. Many studies, like Luksch *et al.* (2016) and Eleveld *et al.* (2015), have revealed that the presence of genetic alterations amplifies tumor growth and progression, resulting in a therapy-resistant relapse. For example, the activation of the YAP gene (*Yes Associated Protein)* and increased overload of mutations in the RAS pathway are major events associated with tumor progression, also providing chemo-resistance to tumor cells (Schramm *et al.*, 2015).

In this scenario, Verteporfin (VP), a small, hydrophobic, and fluorescent porphyrin, has been recently identified as an inhibitor of the YAP/TAZ-TEAD complex, providing positive anti-cancer results in different tumor types, including NB (Fusco *et al.* (2021)).

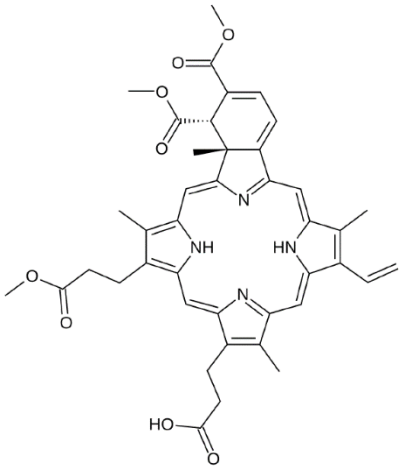

Figure 1.30 *Molecular structure of Verteporfin.*

Thus, the pharmacological inhibition of YAP/TAZ using VP could represent a potential approach for NB therapy.

1.4 Extracellular vesicles

Extracellular vesicles (EVs) are small-sized vesicles (30-10000 nm in diameter), of endocytic origin, released by many types of cells under both normal and pathological conditions. They are characterized by a phospholipid bilayers membrane and contain principally miRNA, ncRNA, DNA double strands, lipids, and proteins highly representative of the cell and tissue of origin. Many studies have revealed that once EVs are released into the extracellular space, they can interact with the matrix, influence the microenvironment, and circulate inside body fluids such as blood, urine, bile, and breast milk. As described by Xu *et al.* (2018), EVs can be internalized by recipient cells through mechanisms like endocytosis mediated by receptors, clathrin-dependent, caveolae-dependent, and lipid raft-dependent.

1.4.1 The role of EVs in cancer detection

As anticipated in paragraph §1.3, the involvement of EVs in physiological processes, including blood coagulation, immunity, differentiation, tissue regeneration, and angiogenesis, has recently become clear. However, as explained in Bebelman *et al.* (2018), cancer cells secrete higher amounts of EVs with respect to non-malignant cells: the release is influenced by microenvironment conditions (pH, hypoxia, exposure to proteins) as well as their cargo. According to Kosaka *et al.* (2014), nanovesicles from tumor cells, once

internalized by another cell, can transfer oncogenic proteins, miRNAs and transcription factors, modifying the surrounding environment with the subsequent proliferation of the tumor. For example, high content of angiogenic factors in EVs induces vascular growth by increasing the transport of nutrients to tumor cells, such as iron and oxygen, with the end cause of tumor spread.

In addition, EVs can activate fibroblasts, resulting in extracellular matrix degradation and cancer-promoting cytokines production. The infiltration of nanovesicles into bone marrow cells, on the other hand, leads to the growth of a pre-metastatic niche. Lastly, EVs may affect the spread of cancer through metastatic sites: an example is given by Peinado *et al.* (2012) who proved the metastasis appearance in educated bone marrow by metastatic melanoma. The phenomena mentioned above can be observed in Figure 1.13.

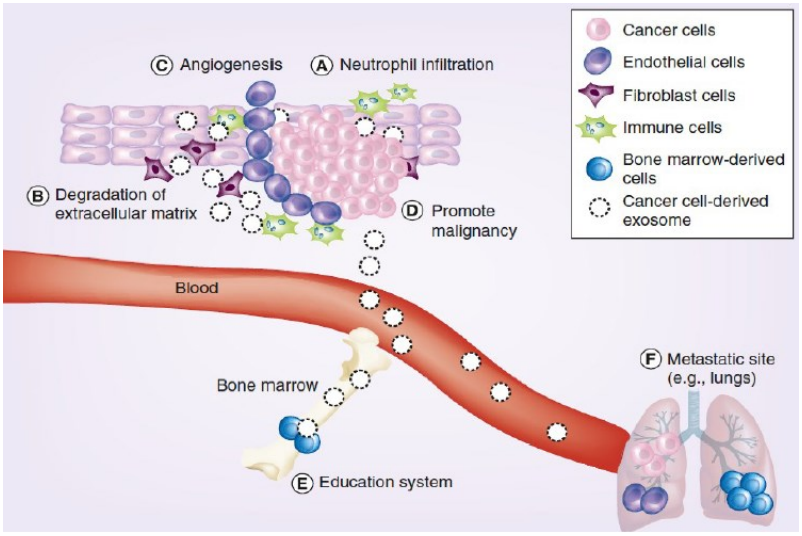

Figure 1.31 *Effects of EV release from cancerous cells on the microenvironment (Kosaka et al., 2014).*

Nevertheless, new medical frontiers are focusing on EVs properties for cancer detection and new therapy approaches.

Concerning cancer detection, EVs could potentially work as biomarkers: Möller & Lobb (2020) reported that liquid biopsy could be performed on body fluids, where the EVs circulate, to provide some information about the disease.

On the other hand, one more interesting application of EVs regards the therapeutic field: they seem to have good properties to be employed as drug delivery systems.

1.4.2 EVs as drug delivery systems

As illustrated in the work of Walker *et al.* (2019), despite the progress granted by chemotherapy in cancer treatment, it has certain drawbacks related to rapid clearance, poor bioavailability, low intra-tumoral delivery, unspecific cytotoxicity, and consequent systemic

effect. To overcome these issues synthetic or natural carriers can be used to deliver the interested drug, showing fascinating results in pre-clinical tests. Among the natural carriers, there are liposomes and EVs.

As summarized in Figure 1.14 from Zhu *et al.* (2018), EVs represent the most promising kind of natural carriers to deliver drugs especially due to their long circulation half-life, their high biocompatibility, their capability to protect and prevent the cargo from enzymatic degradation, their high penetration through barriers, and especially their capability of targeting specific cells and tissues. Some other advantages concern the exhibition of low immunogenicity and the aid of cell regeneration and differentiation.

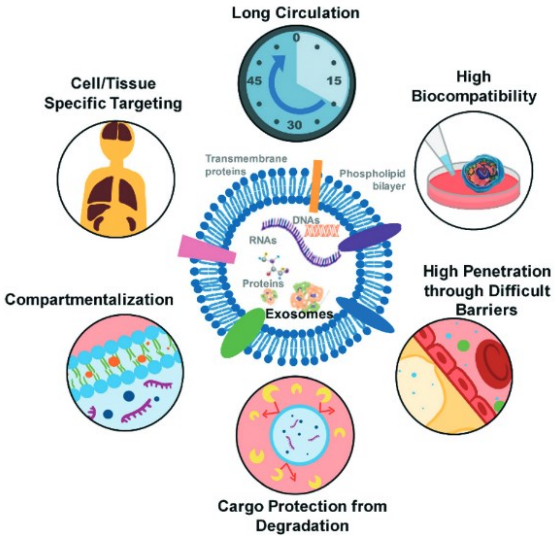

Figure 1.32 *Advantages in the use of EVs as natural drug carriers (Zhu et al., 2018).*

Many techniques are available to engineer EVs. As described by Zhu *et al.* (2018), the main approaches are:

- Surface molecular engineering;
- Membrane permeabilization-mediated cargo loading.

The surface molecular engineering method is based on EVs surface modification through donor cell manipulation, receptor-ligand binding, or covalent binding. Advantages and disadvantages are shown in Figure 1.15.

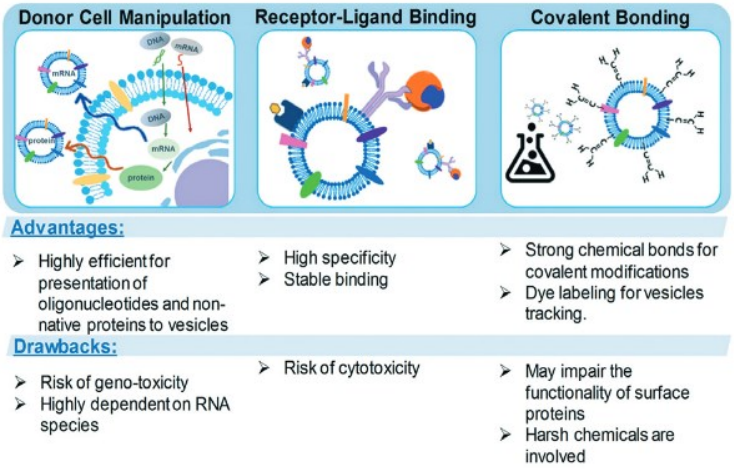

Figure 1.33 *Scheme of the different strategies for surface engineering of EVs (Zhu et al., 2018).*

The membrane permeabilization method is used to facilitate the passage of hydrophilic molecules across the EVs membrane, using physical or chemical active loading strategies. In Figure 1.16 the different mechanisms are summarized.

According to Walker *et al.* (2019), among the physically-induced mechanisms, electroporation, sonication, freeze and thaw cycles, and extrusion are the most common procedures, in which an external force disrupts EVs membrane, allowing the diffusion of the molecule of interest. For instance, in electroporation, the application of an electric field induces the spontaneous formation of pores in the bilayer membrane.

Concerning the chemically-induced mechanisms, chemical agents such as saponin and transfection reagents have particular importance. For instance, saponin selectively removes membrane cholesterol and opens pores.

Finally, the encapsulation of hydrophobic molecules within EVs can be mediated by simple incubation, owing to the hydrophobic nature of the EVs membrane.

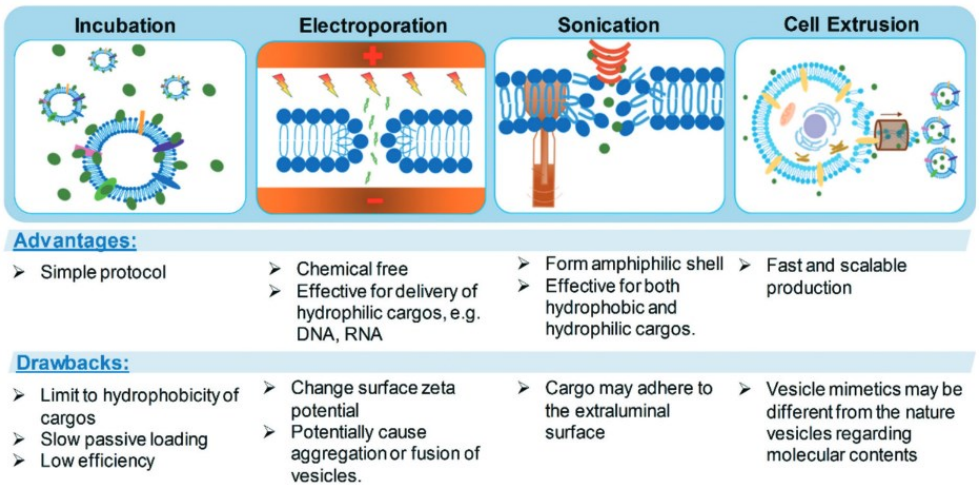

Figure 1.34 *Scheme of the different mechanisms for membrane permeabilization of EVs (Zhu et al., 2018).*

1.4.3 MSC-derived EVs

EVs can be isolated from many sources, including immune cells, cancer cells, and mesenchymal stem cells (MSCs). A detailed description of the principal sources together with their respective advantages and disadvantages is reported in Walker *et al.* (2019).
Immune cells are a particularly promising source of EVs for cancer therapy, as immune-derived EVs contain cytotoxins capable of cancer death.
Cancer cells produce a large amount of EVs characterized by an intrinsic homing ability, and capable of overcoming the drug resistance of stem cell-like cancer cells. However, their main issue concerns the possibility of introducing molecules into the recipient cells that could promote the activation of pathological pathways. A method could be developed to deactivate and/or remove the harmful content of EVs, but it would make the entire drug loading process more complex.
MSCs, multipotent stem cells found in the bone marrow and adipose tissue, are the most promising source of EVs. Bebelman *et al.* (2018) state that MSCs inhibit cancer proliferation: due to their intrinsic therapeutic property, they can be exploited for transferring therapeutics to tumors using MSCs-derived EVs as vehicles. Moreover, based on a preclinical model, Giebel *et al.* (2017) have evidenced that the immunomodulating factors of MSCs are also secreted *ex vivo* and reside in the EVs secreted by these cells.

1.5 Motivation and aim of the thesis

Despite being the guilty part of cancer progression and metastasis, EVs could potentially be used to our clinical advantage by transforming them into drug delivery systems.
Although traditional methods for EVs modifications will continue to play a significant role in the future, microfluidic approaches will eventually replace benchtop methods for investigating EVs in speeding up precision therapeutics.
Considering such promises, the goal of the project is to design and develop a microfluidic device for generating drug-loaded EVs. EVs can be loaded with various therapeutic agents, including VP. Taking advantage of *lab-on-chip* devices, passive VP-loading through microfluidic mixing and incubation may be an important strategy to produce functional engineered EVs.
The platform is designed using AutoCAD® and modelled with COMSOL Multiphysics® so that both a perfect mixing between EVs and VP occurs within the mixing unit and the desired incubation time is achieved. The master mold is fabricated with photolithography, and PDMS replicas of the chips are obtained with replica molding processes. Plasma treatment is used to form an irreversible hydraulic seal of the microfluidic platform to a glass support. The platform in this configuration is used to perform both fluid dynamic and biological validations.

Chapter 2

Materials and methods

This second Chapter deals with the main procedures and protocols optimized during the project. Firstly, the design of the platforms, also exploiting COMSOL Multiphysics® for the fluid dynamic simulation, and the methods to produce the masters are presented. In the following, the procedures to validate the platforms are illustrated. Finally, biological protocols and biological experiments needed for the assessment of VP-loading inside EVs are described.

2.1 Microfluidic platforms

The design of the microfluidic platform for generating drug-loaded EVs is grounded on the procedure published by Fuhrmann *et al.* (2015).
Specifically, the standard procedure calls for MSC-derived EVs to be mixed with different porphyrins and for passive loading to be performed with a 10-minute incubation time.
Based on this standard procedure, the microfluidic device is designed to allow mixing and incubation to produce engineered functional EVs in a single chip. In the following, the description of the geometry and the fabrication procedure of both the master and the device is given. Furthermore, the fluid dynamic simulation tool is explored.

2.1.1 Design of the platform

The microfluidic platform is designed in AutoCAD® using 2D and 3D environments. In Figure 2.1 the platform design is shown with all the dimensions reported. The device, characterized by a T-type inlet channel, consists of two sections: a mixing unit, where the two fluids entering the platform are mixed until perfect homogeneity, and an incubation unit designed to guarantee the incubation time of 10 minutes provided by Fuhrmann *et al.* (2015).
Once injected from the inlets, the fluids meet and flow into a 0.2 mm wide and 1.7 mm long channel feeding the mixing unit, which consists of a micromixer with five mixing units 0.5 mm wide and 0.5 mm long, for a total length of 2.5 mm. The geometry of the micromixer is adapted from Fang *et al.* (2012), where obstacles have a thickness of 50 μm and a rotation angle of 69°.
The incubation unit comprises delay-lines 300 mm long and 0.7 mm wide. The height of all elements is 0.1 mm ensuring a width-to-height ratio larger than 1:10 and smaller than 10:1, which avoids the collapse of the structure during soft lithography processes.

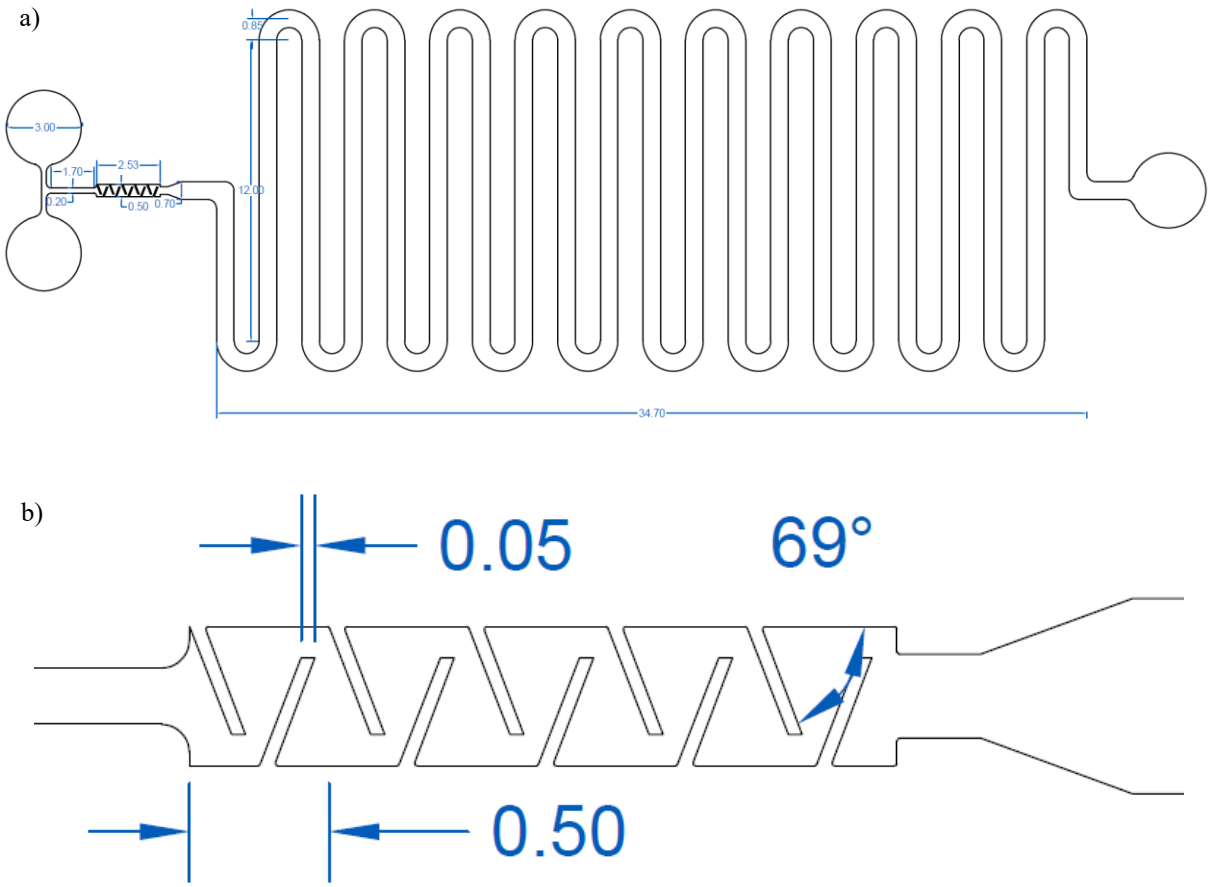

Figure 2.35 *Platform layout: a) AutoCAD® design of the platform; b) detail of the micromixer. All dimensions are in mm.*

The length of the delay-lines is determined according to Equation 1.16, knowing the velocity measurement at the end of the mixing unit, dependent on the initial flow rate, and the height and width of the delay-lines.

To optimize the geometry of the micromixer and solve issues related to air bubbles formation inside the micromixer, the platform is revised to:

- Round all edges;
- Modify obstacles by adapting the geometry from Yuan *et al.* (2022).

The reviewed geometry consists of a Y-type inlet channel, a mixer unit, and an incubation section, as shown in Figure 2.2 with all the dimensions. Specifically, the mixing unit now consists of a micromixer with angled obstacles composed of two parts, one longer than the other measuring 0.24 mm and 0.2 mm, respectively, angled at 122°.

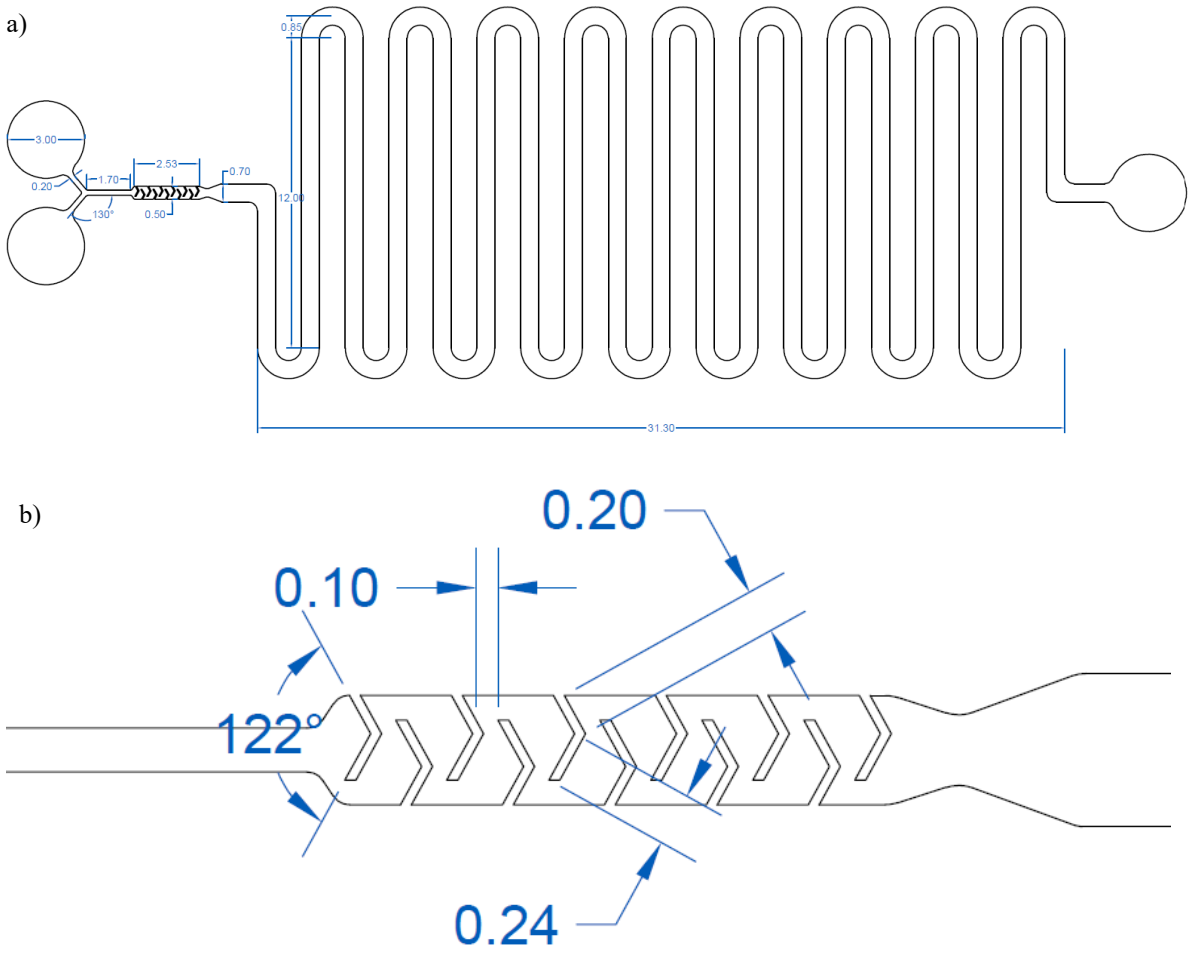

Figure 2.36 *Platform layout: a) AutoCAD® design of the reviewed platform; b) detail of the micromixer. All dimensions are in mm.*

The width-to-height ratio falls within the optimal range and the delay-lines length of 264 mm is adapted to the new velocity at the end of the mixing unit.

2.1.2 COMSOL Multiphysics® simulation

Computational Fluid Dynamics (CFD) is an important tool capable of numerically solving balance equations to analyze fluid flow behavior in a domain. CFD uses the *Finite Volume Element*, a numerical technique that leads to domain discretization so that a mesh is produced. The mathematical model, generally a Differential and Algebraic Equations system (DAEs), is transformed into an Algebraic Equations system (AEs) which is solved in each mesh element and then checks if the numerical solution is approximately equal to the DAEs solution.

COMSOL Multiphysics® is a CFD software, organized into modules representing different physics that can be added to the system. For the goal of the project, the physics examined are:

- Laminar flow of a single-phase incompressible fluid to describe the fluid motion;
- Transport of diluted species to simulate the diffusive behavior of a generic species i.

The results of the simulation are compared with the experimental data to validate the proper operations of the platform.
To set up the simulation, the 3D geometry designed in AutoCAD® is first imported into COMSOL Multiphysics®. The fluid inside the platform is assumed to be water since its physical properties are comparable to the ones of the solutions experimentally used. A normal mesh with default elements is created and both *steady-state* and *time-dependent* simulations are performed. In the latter case, the platform behavior is investigated between 0 and 30 minutes to verify, especially for the transport of diluted species, the correct incubation time.

2.1.2.1 Laminar flow

The laminar flow of a single-phase fluid is described by the Navier-Stokes equations composed of conservation of mass, momentum, and energy. To solve them, the fluid is considered Newtonian, with constant density at constant temperature, and no-slip conditions are applied to the wall. To solve the laminar flow physics some parameters have been defined:

- Temperature of 20°C;
- Inlet mass flow rates of 1 μL/min;
- Outlet pressure of 0 Pa.

2.1.2.2 Transport of diluted species

The transport of a diluted species permits the description of the movement of chemical species by diffusion and convection in a defined domain. The species are assumed to be diluted, meaning that the fluid properties are those of the solvent.
In the designed platform two aqueous streams enter, containing EVs and VP. To distinguish the two fluids, COMSOL Multiphysics® provides the option of identifying a reference component and, depending on its presence or absence, assigning a concentration of 1 or 0, respectively. For this study, EVs are considered the reference substance owing to the lowest diffusion coefficient. In Equations 2.1 and 2.2 the diffusion coefficients referred to EVs and VP are computed exploiting the Einstein-Stokes equation:

$$D_{EVs} = \frac{1.38 \cdot 10^{-23} \cdot 310}{6\pi \cdot 8.9 \cdot 10^{-4} \cdot 70 \cdot 10^{-9}} = 3.44 \cdot 10^{-12} \frac{m}{s} \quad (2.19)$$

$$D_{VP} = \frac{1.38 \cdot 10^{-23} \cdot 310}{6\pi \cdot 8.9 \cdot 10^{-4} \cdot 0.833 \cdot 10^{-9}} = 2.89 \cdot 10^{-10} \frac{m}{s} \quad (2.20)$$

As explained in §1.1.1, in microfluidics the transport of species is governed by diffusion; the solute follows Fick's law and the mass balance of the species i is given by Equation 1.8. While the diffusive term is always included in this module, the convective term is activated by default but can be excluded by the user. For the current study, the convective term is kept active.

Finally, the velocity term is calculated by coupling both physics, *i.e.*, laminar flow with dilute species transport. The parameters defined in this section are:

- Temperature of 20°C;
- Diffusion coefficient of $3.44 \cdot 10^{-12}\ m/s$;
- Inflows normalized concentration (0 or 1).

2.1.3 Production of the master

The master is produced in a clean room following the protocol described below. The main steps are the design of the photomask, pre-treatment of the silicon wafer, deposition of photoresist, soft bake and exposure, post-exposure bake and development, and hard bake. It is important to work in the dark, control humidity, and prevent dust from corrupting the final product.

2.1.3.1 Design of the photomask

To create a negative photomask, the platform geometry designed in AutoCAD® is imported into Adobe Illustrator® to properly color the different areas of the mask. Where the photomask is transparent the photosensitive resin will be exposed to the UV light allowing crosslinking, while black areas will not allow crosslinking of the underlying photoresist layer.

2.1.3.2 Pre-treatment of the silicon wafer

A 10 cm diameter silicon wafer is first rinsed with acetone, methanol, and distilled water, and dried with a clean stream of compressed air. Then, the cleaned silicon wafer is placed inside a desiccator saturated with Hexamethyldisilazide vapors (Sigma-Aldrich®) for 15 minutes to favor the adhesion of the photoresist.

2.1.3.3 Deposition of the photoresist

Once the pre-treatment is finished, the wafer is set on a spin coater (SPS Spin 150 wafer spinner) connected to a vacuum pump. 1 mL of SU-8-2100 negative photoresist (MicroChem) is deposited on the wafer and spin-coated to obtain a thickness of 100 μm following two steps:

- Spin at 500 rpm for 10 seconds with an acceleration of 100 rpm/s;
- Spin at 3000 rpm for 30 seconds with an acceleration of 300 rpm/s.

The wafer is then placed on a flat surface and left to rest for 5 minutes.

2.1.3.4 Soft Bake and Exposure

Consistent with the height of the photoresist layer desired, the wafer is soft baked (SB) on a hotplate at 95°C for 20 minutes, to remove the internal stresses of the material and evaporate solvent traces contained in the photoresist.
Subsequently, the wafer is covered with the photomask and exposed to UV light. The exposure energy (E_{exp}) is set in relation to the thickness of the photoresist, and the corresponding exposure time (t_{exp}) is calculated knowing the lamp power (P) according to Equation 2.3:

$$t_{exp} = \frac{E_{exp}}{P} \qquad (2.\ 21)$$

In this specific case, the exposure time is 48 seconds with an energy of 240 mJ/cm^2.

2.1.3.5 Post Exposure Bake and Development

The Post-Exposure Bake (PEB) is a heat treatment that allows complete cross-linking of the photoresist. Again, treatment conditions depend on the desired layer thickness. For our master, the silicon wafer is placed on a hotplate at 95°C for 10 minutes.
The development process removes all the not cross-linked polymer by immersing the wafer in a beaker filled with a solvent, propylene glycol monomethyl ether acetate (Sigma-Aldrich®), for 10 minutes, and dried with compressed air.

2.1.3.6 Hard Bake

Another heat treatment, Hard Bake (HB), improves the mechanical and thermal characteristics of the master. The wafer, covered with aluminum foil, is placed on a hot plate and the following steps are set:

- Temperature of 65°C for 10 minutes;
- Temperature ramp from 65°C to 160°C with a rate of 120°C/h for 2 hours.

2.1.4 Production of the platform

The PDMS platform is produced using replica molding and plasma treatment. As explained in §1.2.2.2, replica molding is a soft lithographic technique that exploits the master and a polymer to reproduce replicas of the device, while plasma treatment permits to form a perfect hydraulic seal between the PDMS microfluidic platform and a glass slide.
Before replica molding, the surface of the master mold is treated with chlorotrimethylsilane vapors (Sigma-Aldrich®) for at least 1 hour to preserve the integrity and definition of the channels and favor PDMS detachment from the master.

2.1.4.1. Replica molding

PDMS Sylgard® 184 (Dow Corning), a two-part kit provided with a silicon elastomer base and a curing agent represented in Figure 2.3, is used for the platform fabrication.

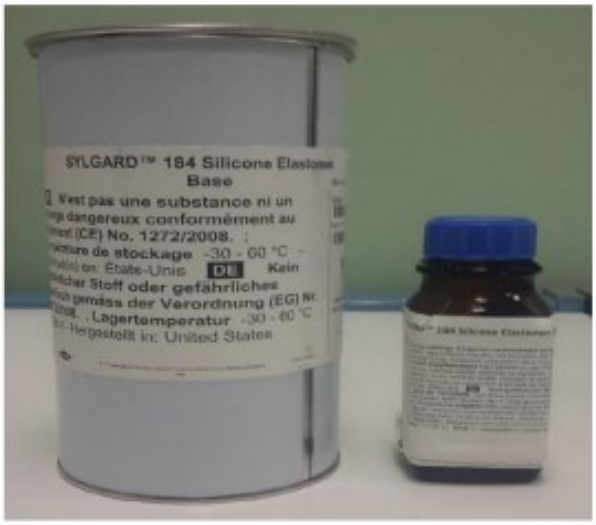

Figure 2.37 *PDMS Sylgard® 184 (Dow Corning), two-part kit: silicone elastomer base on the left, curing agent on the right*

The steps of the replica molding process are:

- Weight the elastomer and the curing agent in a proportion of 10:1 inside a plastic cup;
- Mix energetically the solution until the formation of a homogeneous solution. During this step, a large number of air bubbles is formed inside the mixture;
- Put the mixture in a desiccator, shown in Figure 2.4, connected to a vacuum pump to remove air bubbles. This step is repeated many times until the solution is clear;
- Pour the PDMS mixture on the master and place it again in the desiccator for additional bubble removal;
- Cure the PDMS on the master inside an oven at 80°C for 45 minutes;

– Remove the cured PDMS from the master.

Figure 2.38 *Desiccator connected to the vacuum pump used in the BIAMET Laboratory.*

Before plasma treatment, the obtained platform is redefined by cutting off the excess PDMS around the geometry. Finally, inlets and outlet are created with the help of a biopsy punch with a diameter of 1 mm.

2.1.4.2. Plasma treatment

As explained in §1.2.3, plasma treatment guarantees a perfect hydraulic seal between the PDMS device and the glass slide through the formation of Si-O-Si covalent bonds. The main steps are:

- Clean the device and the coverslip (60x40 mm) from any residues with scotch tape;
- Insert them inside the Plasma Cleaner (PDC-002-CE by Harrick Plasma) chamber shown in Figure 2.5 (a), and close both the door and the valve. The surfaces to be activated must be faced upwards;
- Switch on the vacuum pump to create vacuum inside the chamber;
- After 4 minutes the plasma is turned on and once a dull pink appears, the valve must be regulated to obtain an intense pink color, as represented in Figure 2.5 (b). This correlates with the ideal percentage of oxygen to promote a good surface activation;
- After approximately 1 minute both the plasma and the vacuum pump are switched off and the valve is slowly opened to restore the atmospheric pressure;
- Put the two pieces in conformal contact, allowing the formation of covalent bonds;
- Place the microfluidic platform in an oven for 5 minutes at 80°C to strengthen binding.

a b

Figure 2.39 *Plasma treatment: (a) plasma Cleaner by Harrick Plasma used in BIAMET Laboratory; (b) color of plasma when an adequate quantity of oxygen is present in the chamber.*

2.2 Platform validation

Platform validation is an important step in the study as it provides insights into whether the device is functioning properly. Specifically, both fluid dynamic and biological validation are performed. Finally, experiments are carried out to verify the presence of VP within the EVs, which are discussed in §2.4.

2.2.1 Fluid dynamic validation

Fluid dynamic validation is accomplished by employing both colored and fluorescent tracers. Colored tracers are food coloring solutions prepared by simply diluting them with water until an intense color is obtained. Fluid dynamic validation can be performed either by direct injection of the solutions with a micropipette or by using a syringe pump.

The fluorescent tracers used are fluorescein isothiocyanate dextrans (Sigma-Aldrich®) with a maximum excitation at a wavelength of 490 nm and maximum emission at 520 nm, available in distinct classes based on different average molecular weights. Each dextran is characterized by a different diffusion coefficient value so that different solutes can be simulated. Since VP has a molecular weight of 718.8 KDa, the 500 KDa category of dextrans are used during validation. The isothiocyanate-dextrans are prepared by mixing them in water at a proportion of 0.0005 g/10 mL. Using dextrans it is possible to observe the specific geometry of the platform under a fluorescent microscope (Invitrogen™ EVOSTM FL Cell Imaging System by Thermo Fischer Scientific, shown in Figure 2.6), using a GFP fluorescence filter at 10x magnification. In this case, one inlet of the platform is blocked with a blind needle, while the solution of dextran is injected from the other inlet with a micropipette.

Figure 2.40 *Invitrogen EVOSTM FL Cell Imaging System by Thermo Fischer Scientific used in BIAMET Laboratory.*

If a syringe pump is used, syringes are filled with colored tracers connected by tubes to each inlet of the platform. Once placed on the pump, it is started at the desired flow rate. The pump PHD Ultra (Harvard Apparatus), in Figure 2.7 (a), is made of a central body and a mechanical multi-rack remote unit. The first has a display to set up process conditions such as the brand and capacity of syringes, flow rate, and mode of operation, namely infusion or withdrawal. The connected remote unit houses the syringes.
The steps for the validation of the platform are:

- Fill the platform with physiological solution to remove any air bubbles;
- Prepare three microtubes to be inserted at both the inlets and the outlet. 21G steel dispensing tips (DRIFTON) are inserted inside the microtubes (inner diameter 0.5 mm, outer diameter 1.5 mm, TYGON® TUBING) of 12 cm length;
- Prepare two 1 mL BD Plastipak™ syringes filled with different colorant solutions, connect them to the microtubes and place them on the pump;
- On the display set the brand of the specific syringes *(BD plastic syringe)*, the capacity *(1 mL)* and the desired flow rate (*1 µL/min)*;
- Start the pump and once the first drops exit from both the dispensing tips, they can be inserted into the platform inlets.

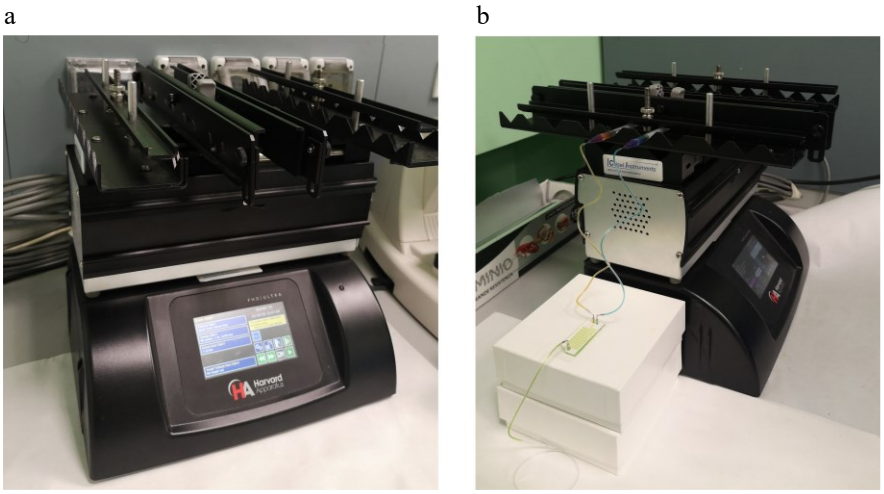

Figure 2.41 *Fluid dynamic validation: a) pump PHD Ultra by Harvard Apparatus employed in BIAMET Laboratory; b) validation process.*

This validation can be helpful to compare the results with the COMSOL Multiphysics® simulations concerning the effectiveness of the mixing section and the time required for the fluid passage through the incubation unit.

2.2.2 Biological validation

As anticipated, biological validation is aimed at verifying the correct loading of the drug into the EVs using the microfluidic chip. Before biological validation can begin, the chip and microtubes must be autoclaved (Europa B Evo, Arco Scientifica) to ensure sterility, and all necessary solutions must be prepared in a bio-safety cabinet.

In particular, VP stock solution (Sigma-Aldrich®) is prepared by diluting the VP powder concentrated 5 mg with Dimethylsulfoxide (DMSO; Sigma-Aldrich®) to a final concentration of 10 mM, while VP working solution is prepared by diluting VP with PBS to a final concentration of 1 mM in a final volume of 200 µL. Approximately 10^9 MSC-derived EVs, previously isolated and characterized, are diluted with PBS to a final volume of 200 µL.

Some precautions need to be taken before starting the actual experiment. First, all the operations are carried out in the dark since VP is sensitive to light; the platform is filled with PBS to remove air bubbles and a 15 mL Falcon tube, used to collect fluids at the outlet, is filled with 10 mL of PBS and placed on ice in order to preserve the integrity of the drug-loaded EVs.

Once the syringe pump is set up as explained in §2.2.1, the experiment can begin.

The experiment can be divided into three steps, each characterized by a different flow rate:

- Replacement step where the PBS present in the platform is replaced to reduce possible undesirable diffusion and dilution of both the VP and the EVs using a flow rate of 5 µL/min;
- Experimental step carried out at the flow rate of 1 µL/min;

- Washing step in which, once the syringes are emptied, they are refilled with 100 µL of PBS and the pump is restarted with a flow rate of 5 µL/min.

Once the experiment is finished, the 15 mL Falcon tube with the samples mixed and diluted with PBS is further ultrafiltrated at 3000 G for 10 min using a 20 mL Spin-X (Corning® Spin-X® UF 20 mL Centrifugal Concentrator) to separate the EVs loaded with VP from the free VP. Finally, the VP-loaded EVs are aliquoted and stored at -80°C until use.

2.3 Biological protocols

This section describes in detail the biological protocols related to cell maintenance, isolation of EVs and the techniques used to characterize them.

2.3.1 Cell lines

Mesenchymal Stem cells (MSCs) and a NB cell line (SK-N-AS) are used to perform the biological validation of the microfluidic device and further biological experiments. Cells used for these applications are provided by ATCC.

2.3.1.1 MSC cells

MSCs are multipotent cells, that can differentiate into different cell types such as osteoblasts, chondrocytes, myocytes, and adipocytes. MSCs are found in bone marrow, umbilical cord cells, adipose tissues, and amniotic fluid. This cell line is used as a source of EVs because of its intrinsic therapeutic properties.

2.3.1.2 SK-N-AS cells

SK-N-AS cell line derives from the bone marrow metastasis in a child with poorly differentiated embryonal NB. These cells are used as target cells for biological analyses.

2.3.2 Cell maintenance, splitting, and counting

Cells are generally seeded in flasks (Corning™) of either 75 cm^2 or 150 cm^2 and kept in an incubator at a temperature of 37 °C and 5% of CO_2 humidity. Each cell line grows in a specific culture medium that provides nutrients for their growth.

For MSCs the medium is prepared using:

- 90% $_{v/v}$ MesenCult™ MSC Basal Medium (Stemcell™);
- 10% $_{v/v}$ MesenCult™ MSC Stimulatory Supplement (Stemcell™), serum-containing supplement optimized for the expansion MSCs,
- 1% $_{v/v}$ Penicillin/Streptomycin (P/S), an antibiotic mixture to prevent bacteria contaminations (CORNING);

- 1% $_{v/v}$ L-Glutamine, an essential amino acid that serves as a major energy source for cells in culture (Corning^{TM}).

For SK-N-AS line the medium is prepared using:

- 90% $_{v/v}$ Dulbecco's Modified Eagle Media (ATCC);
- 10% $_{v/v}$ Fetal Bovine Serum (ATCC);
- 1% $_{v/v}$ Penicillin/Streptomycin;
- 1‰$_{v/v}$ MEM Non-Essential Amino Acids (Gibco^{TM}) used as a supplement for cell culture medium to increase cell growth and viability

Once the flask reaches a confluence of about 70-80%, cells must be subcultured by a procedure of splitting, which consists of the periodic separation of the cell population. The purpose of cell splitting is to prevent growth arrest and ensure survival.
The degree of subculturing a cell line has undergone is often expressed as "passage number", which can generally be thought of as the number of times cells have been transferred from flask to flask. The MSCs used to isolate EVs are from passage number 1 to 8 as recommended by a growing body of literature, including Fuhrmann *et al.* (2015) and Patel *et al.* (2017) studies, indicating these as the optimal conditions for using MSC-derived EVs as drug delivery systems.
With regards to cell splitting, the procedure is carried out under a bio-safety cabinet, that preserves sterility. Before starting, both culture medium and Trypsin/EDTA (Sigma-Aldrich®) solution are warmed to 37 °C. Then, the protocol can be started:

- Remove the medium from the old flask with a 10 mL serological pipet and store it in a 15 mL Falcon tube;
- Rinse gently the flask with approximately 4 mL of PBS (Gibco^{TM}) to remove any trace of culture media that contain Trypsin inhibitors. Then PBS is aspirated and discarded;
- Add 2 mL of Trypsin, an enzyme capable to detach cells from the flask surface, verifying that all the flask bottom surface is covered by the solution, and place the flask at 37°C in a CO_2 incubator for approximately 3 minutes;
- Verify the detachment of the cells with the microscope;
- Add the old medium inside the flask to inhibit the action of the Trypsin. The solution of cells is pipetted until the achievement of homogeneous cell suspension and place and placed in a 15 mL Falcon tube;
- Count cells using the Bürker Chamber
- Centrifuge the cell suspension at 1600 rpm for 10 minutes with soft deceleration to induce the sedimentation of cells;

- Once the centrifugation is ended, the supernatant is discarded, while the pellet of cells is resuspended in a small amount of fresh medium;
- Prepare the new flask by adding 10 mL of medium and an aliquot of the resuspended cells;
- Incubate the flask at 37°C and 5% CO_2.

The quantities of reagents reported are related to the splitting of a 75 cm^2 flask; for the 150 cm^2, all the volumes should be doubled.
To count cells and calculate cellular concentration the Bürker chamber is used; as represented in Figure 2.8, it is formed by a rectangular slide with a chamber engraved with a laser-etched grid, and a 9x9 mm^2 coverslip. The grid has nine squares, each delimitated by three parallel lines. When the slide and the coverslip are assembled, a chamber of 1/10 mm^3 is created, and cell counting is executed for each of the 9 squares. Specifically, the protocol is:

- Mix 10 µL of Trypan Blue (Invitrogen™), a cell stain that colors dead cells in dark blue, with 10 µL of the cell suspension to be counted;
- Insert 10 µL of the mixture inside the chamber by capillary force;
- Count the number of live cells (bright dots) in each square, observing the chamber at the microscope with a 10x enlargement;
- Calculate the arithmetic mean of cells per square.

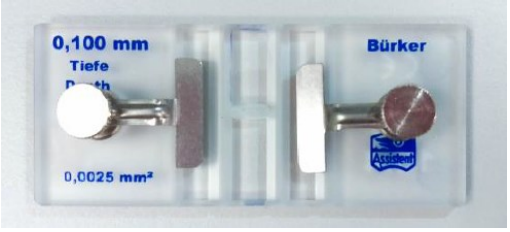

Figure 2.42 *Bürker chamber.*

Finally, cell concentration can be computed using Equation 2.4:

$$N_{cell} = N_{average} \cdot d_1 \cdot V_f \cdot K \qquad (2.22)$$

Where d_1 is the dilution factor of the cells equal to 2, V_f is the volume of medium in which the cells are suspended, and K is the Bürker Chamber constant, equal to 10000, related to its geometry and volume (number of squares per mL).

2.3.3 EVs isolation

EVs are isolated from the Conditioned Medium (CM) by the ultrafiltration technique. The procedure requires the following steps:

- Seed $4.5 \cdot 10^5$ cells in a T150 flask in complete growth medium and incubate at 37°C and 5% CO_2;
- After 72 hours, replace the medium with 20 mL of MesenCult™ MSC Basal Medium supplemented with 1% P/S and 1% L-Glut without MesenCult™ MSC Stimulatory Supplement to avoid interference by EVs that might be present in the serum;
- After 48 hours, remove the medium, now called CM, with a 25 mL serological and place it in a 50 mL Falcon tube;
- Centrifuge for 5 minutes at 500 G imposing soft deceleration to remove cellular debris and filter the supernatant with 0,22 μm filters (Sartorius);
- Load the CM in a 20 mL Spin-X and centrifuge for 30 minutes at 3000 G;
- Wash the Spin-X with 13 mL of PBS, and centrifuge again for 15 minutes at 3000 G;
- Collect EVs and either use them fresh or store them at -80 °C for future characterization and experiments.

2.3.4 EVs characterization

Once the EVs are isolated, a key step is to characterize them to yield information about their size, concentration, and protein content. Here, we discuss the techniques that have been employed: *Bicinchoninic Acid Protein Assay* (BCA), *Nanoparticle Tracking Analysis* (NTA), *Western Blot* (WB) and *Transmission Electron Microscopy* (TEM).

2.3.4.1 Bicinchoninic Acid Protein Assay

The BCA Assay is a technique used to quantify the total amount of proteins in EVs. For this assay, the Pierce™ BCA Protein Assay Kit is employed. The colorimetric analysis is based on two reactions:

- Chelation of copper with protein in an alkaline environment, leading to the formation of a blue-colored complex (biuret reaction);

$$protein + Cu^{2+} \xrightarrow{OH^-} Cu^{+} \tag{2.23}$$

- Reaction between BCA and cuprous cation previously produced forming a purple color.

$$Cu^{+} + 2BCA \longrightarrow$$ 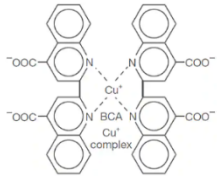 (2.24)

The BCA-copper complex is water soluble and absorbs at 562 nm with increasing protein concentration. Absorbance is measured at 562 nm by Tecan Microplate Reader Spark.

2.3.4.2 Nanoparticle Tracking Analysis

NTA is used to characterize nanoparticle suspension, by assessing their size and concentration. NTA analyses are performed with NanoSight NS300. In particular, the system is formed by a microfluidic chamber and a laser arrangement with a 20x microscope objective connected to a camera. EVs injected into the chamber are hit by a beam and scatter the laser light, which is collected in the microscope; a camera captures videos where the Brownian motion is shown. Finally, NTA software (NTA 3.4 Build 3.4.4) performs a particle-by-particle analysis. Using NTA, it is possible to compute EVs hydraulic diameter and concentration. The NTA instrument arrangement and the detail of the microfluidic chamber are represented in Figure 2.9.

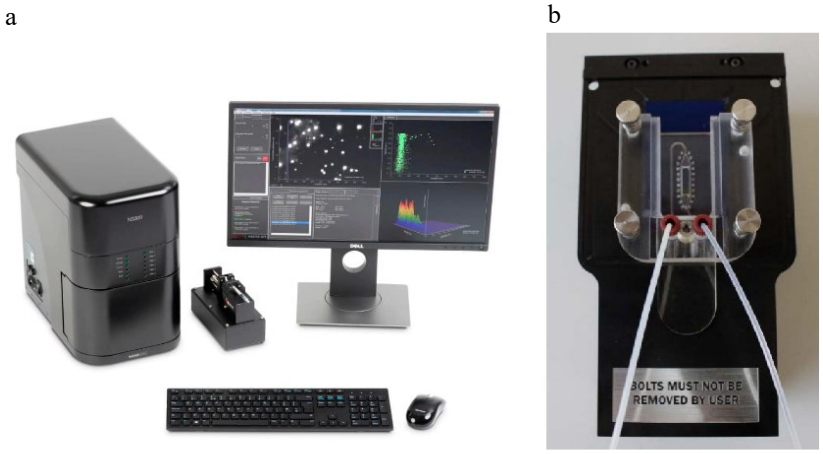

Figure 2.43 *NTA instrumentation: a) Nanosight ns300; b) detail of the microfluidic chamber.*

2.3.4.3 Western Blot

Western Blot (WB) is a biochemical technique that leads to the identification of a particular protein in a protein mixture by specific antibodies. The assay uses sodium-dodecyl sulfate-polyacrylamide gel electrophoresis (SDS-PAGE) to separate proteins according to their molecular weight. The proteins are then transferred from the gel into a nitrocellulose membrane, where they are recognized and bound with the related antibodies. As a result, a given protein contained in a sample can be identified and quantified.

Although there are no specific markers for the identification of EVs, it is possible to take advantage of specific known surface proteins among which the most widely used is CD63,

a cell surface glycoprotein. Calnexin is used as a negative control, given its absence in EVs. Images are acquired using iBright Western Blot Imaging Systems (Invitrogen™).

2.3.4.4 Transmission Electron Microscopy

TEM is a microscopy technique in which an electron beam is transmitted through the sectioned sample to produce a highly resolved image for visualizing the internal structures of an element. For the characterization of EVs, samples are subjected to a special staining technique known as Immunogold. The operation is similar to the indirect Immunofluorescence method: the colloidal gold particles are conjugated to the secondary antibody, which in turn binds to the primary antibody, the anti-CD63 antibody.
The samples are observed with a Tecnai G2 transmission electron microscope (FEI) operating at 100 kV. Images are acquired with a Veleta digital camera (Olympus Soft Imaging System).

2.4 Biological experiments

Biological experiments are performed to verify the presence of VP inside the EVs and perform preliminary studies on their internalization and therapeutic effects on a NB target cell line.

2.4.1 Nanoparticle Tracking Analysis

NTA analysis is performed to assess the VP-loaded EVs concentration and to verify any difference in EVs size after the loading procedure. The protocol is the same as in §2.3.4.2.

2.4.2 Absorbance and Fluorescence

To evaluate the loading capability of VP within EVs, two properties of the drug are exploited. As explained in §1.3, VP has a characteristic peak of absorbance at 690 nm and emits a fluorescence signal after excitation at 420 nm. Absorbance and Fluorescence scans are generated through the usage of Tecan Microplate Reader Spark.

2.4.3 Immunofluorescence

Immunofluorescence (IF) is a cell imaging technique that relies on the use of antibodies to label specific target antigens with a fluorescent dye, *i.e.* a fluorophore that allows the detection of a wide variety of antigens under a fluorescent microscope. Depending on whether it is conjugated either to the primary or to the secondary antibody, two IF methodologies can be distinguished namely direct or indirect mode, as shown in Figure 2.10.

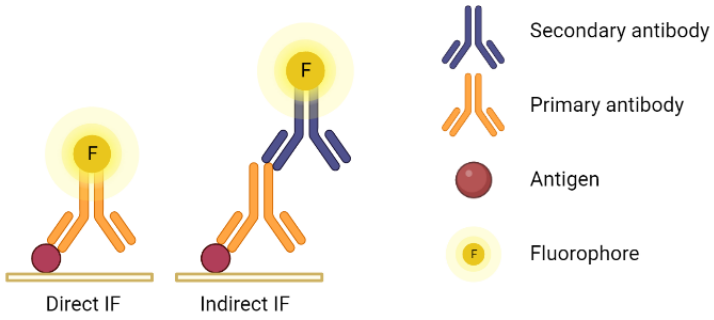

Figure 2.44 *Direct and Indirect immunofluorescence (BioRender.com).*

The indirect method has increased flexibility and signal amplification.

Typically, IF steps usually consist of fixation, permeabilization, blocking and staining. Fixation is commonly accomplished with paraformaldehyde (PFA) to prevent autolysis and preserve morphology while maintaining antigenicity; permeabilization removes cellular membrane lipids, to allow the entrance of larger molecules, as antibodies, and is performed with detergents like Triton X-100; blocking serves to prevent antibodies from binding to non-target epitopes and uses reagents such as Bovine Serum Albumin (BSA). For the aim of the study, the focus is on the analysis of YAP expressions. As explained in §1.3, VP is an inhibitor of the YAP\TAZ complex. Moreover, DAPI (diamidino-2-phenylindole), a blue fluorescent dye represented in Figure 2.11, is also used to stain selectively the nuclei.

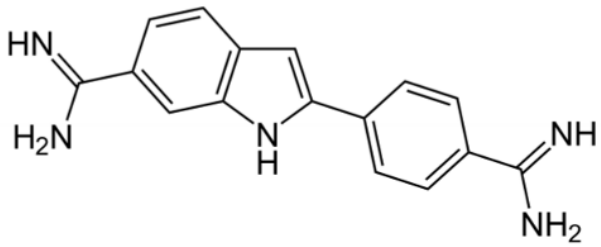

Figure 2.45 *DAPI (diamidino-2-phenylindole) molecular formula.*

The detailed protocol follows:

- Seed $1.2 \cdot 10^4$ cells in each well of an 8 wells chamber slide (Corning™) and allow to adhere at 37°C in a CO_2 incubator;
- After 24 hours, treat the cells under a bio-safety cabinet with an increasing concentration of VP-loaded EVs (1, 5, and 10 μM). Controls are cells treated with the same concentration of free VP and with no treatment;
- Wash cells in PBS three times for 5 min;
- Fix cells in 4% PFA for 15 minutes at room temperature;
- Wash cells in PBS three times for 5 min;
- Permeabilize cells with a 0.1% solution of Triton X-100 for 12 minutes;
- Wash cells in PBS three times for 5 min;
- Add the BSA blocking solution (5% BSA in PBS) for 1 hour at room temperature;
- Incubate cells with the primary antibody (YAP) at 1:1000 overnight at 4°C;
- Wash cells in PBS three times for 5 min;
- Incubate cells with the secondary antibody (Alexa Fluor™, 488 nm anti-rabbit) at 1:800 in PBST for 1 hour at room temperature;
- Add DAPI solution 1:1000 in PBS for 15 minutes at room temperature;
- Wash cells in PBS three times for 5 min;
- Mount the chamber slide onto a glass coverslip by adding 30-50 μL of 90% glycerol;
- Seal the coverslip using nail polish wax to prevent it from moving.

After sealing, the IF samples can be stored upright in a covered slide box at 4°C.
Imaging is performed on a Zeiss LSM800 Airyscan. ImageJ software is used to quantify the fluorescence signal produced respectively by DAPI, YAP e VP according to the protocols published by Jonkman *et al.* (2020) and Mahbubul H. Shihan *et al.* (2021).

2.4.4 MTT assay

MTT assay is a colorimetric analysis for measuring metabolism, and correlates very well with cell viability. From MTT, the half maximal inhibitory concentration (IC_{50}) that represents a value commonly valued in pharmacology to measure the potency of a given agent, can be extrapolated. MTT is based on a metabolic reaction, shown in Figure 2.12, which takes place in mitochondria.

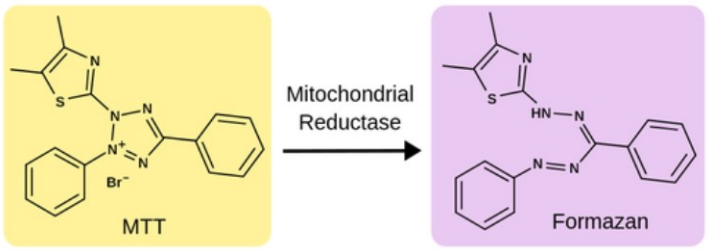

Figure 2.46 *Mitochondrial reductase of MTT reagent towards Formazan (theory.labster.com).*

The reaction involves the reduction of MTT (3-(4,5-dimethylthiazol-2-yl)-2,5-diphenyl-2H-tetrazolium bromide) into formazan, which has a purple color. The more intense the color, the higher the cell viability. We here assessed the effect of VP after 48 hours to compare results with those obtained by Fusco *et al.* (2021). The assay is performed in 96-multiwell plates and involves the following steps:

- Seed $1.5 \cdot 10^4$ cells in 100 µL per well and allow to adhere at 37°C in a CO_2 incubator;
- After 24 hours, treat cells with increasing concentration of either VP-loaded EVs (0.001, 0.01, 0.1, 1 and 10 µM) or free VP for 48 hours at 37°C in a CO_2 incubator. Each concentration is repeated in a duplicate manner. Positive controls consist of no treatment. Negative controls consist of treatments without cells;
- Add 10 µL of MTT solution per well and incubate for 4 hours at 37°C and 5% CO_2;
- Solubilize the formed formazan crystals by adding 100 µL of DMSO per well, including controls;
- Read the absorbance at 570 nm with Tecan Microplate Reader Spark.

Cell viability can be evaluated from the absorbance according to Equation 2.7:

$$\%\ Cell\ Viability = \frac{OD_{exp} - \overline{OD}_{neg-control}}{\overline{OD}_{pos-control} - \overline{OD}_{neg-control}} \quad (2.25)$$

Where OD_{exp} is the measured optical density, $\overline{OD}_{neg-control}$ is the average optical density between the negative controls and $\overline{OD}_{pos-control}$ is the mean between the positive controls. Then cell viability versus drug concentration plot is built so that IC_{50} can be evaluated.

2.4.5 Statistical analysis

Graphs and statistical analyses are performed using GraphPad Prism software. Statistical significance is determined using Student's t-test. Values of $p < 0.05$ (*) are considered statistically significant.

Chapter 3

Results

In this Chapter, the results of the platform design, fluid dynamic simulations, production, and subsequent validations are reported. Finally, preliminary biological results are presented.

3.1 Microfluidic platforms

3.1.1 Design of the platform

In Chapter 2, the geometries of the developed platforms are described. In Chapter 3, the motivations for the platform modifications are discussed.

The platforms consist of a mixing unit and an incubation unit to replicate the standard drug-loading protocol published by Fuhrmann *et al.* (2015). During the use of the first platform, one of the main issues observed concerns the formation of air bubbles in the mixing unit, which slows down and hinders the mixing process. Therefore, some modifications are proposed to improve this unit. Specifically, all angles are rounded to decrease wall effects. In addition, the T-type inlet channel is replaced by a Y-type inlet channel to improve mixing of the two flows, as argued by Udaya Kumar *et al.* (2021). Finally, by introducing and adapting the geometry suggested by Yuan *et al.* (2022), the number of obstacles in the same length of unit operation is increased. The comparison between the two mixing units is shown in Figure 3.1.

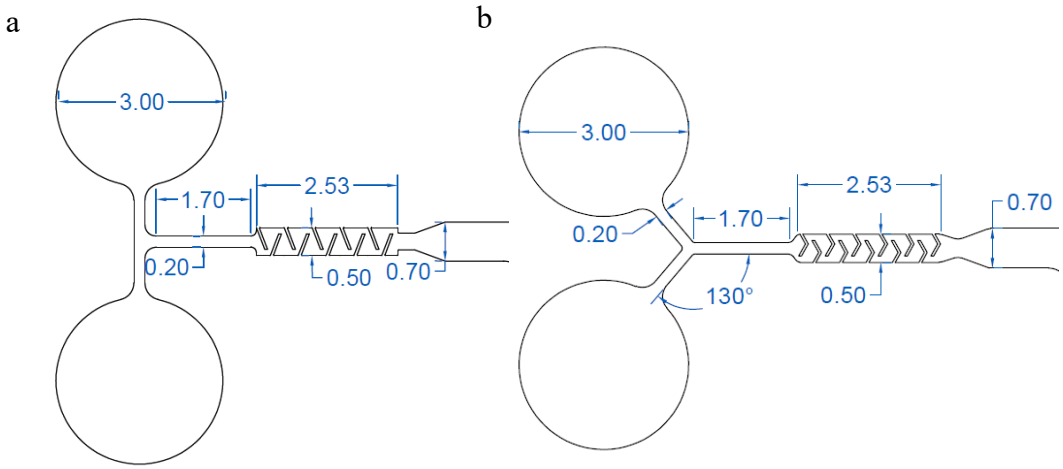

Figure 3.47 *Platform layout comparison: initial section of a) first geometry and b) second geometry. All dimensions are in mm.*

Regarding the incubation unit, the length of the delay-lines is calculated for both platforms through equation 1.16, knowing the required residence time, the height and width of the structure, and the flow rate at the outlet of the micromixer. The latter can be retrieved from COMSOL Multiphysics®, with a tool that returns the average velocity over a defined plane. The calculations are reported:

$$l_{first\ platform} = \frac{10\ min \cdot 60 \frac{s}{min} \cdot 0.5\ \frac{mm}{s} \cdot 0.1 \cdot 0.7\ mm^2}{0.1 \cdot 0.7\ mm^2} = 300\ mm \qquad (3.26)$$

$$l_{second\ platform} = \frac{10\ min \cdot 60 \frac{s}{min} \cdot 0.44\ \frac{mm}{s} \cdot 0.1 \cdot 0.7\ mm^2}{0.1 \cdot 0.7\ mm^2} = 264\ mm \qquad (3.27)$$

As can be noted, the length of the delay-lines is shorter for the revised platform due to the lower velocity at the end of the mixing unit.
Finally, the platforms are exported from the 2D AutoCAD® environment to the 3D environment, as this format is useful for fluid dynamic simulation in COMSOL Multiphysics®. Figure 3.2 shows the two 3D geometries.

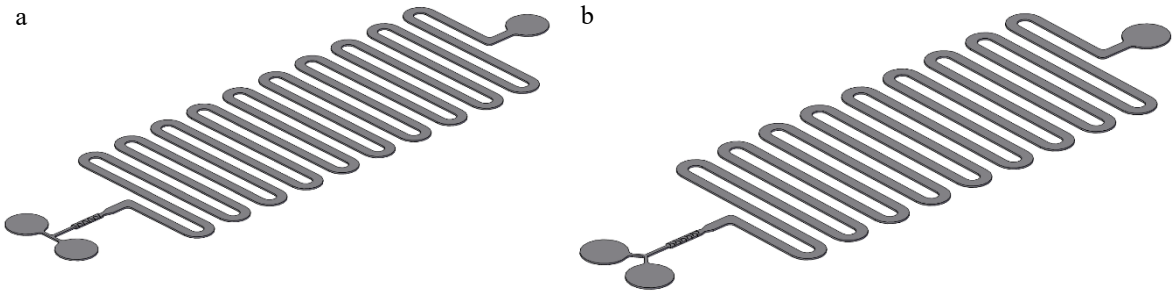

Figure 3.48 *Platform layout: 3D file of a) first geometry; b) second geometry.*

3.1.2 COMSOL Multiphysics® simulation

COMSOL Multiphysics® simulations provide insight into the behavior of fluids within the platform. As explained in §2.1.2, simulations are performed in a 3D environment, importing the AutoCAD® geometry, and both laminar flow and transport of diluted species physics are examined. As simulation results we expect that: the flow is laminar, perfect mixing of the species is obtained at the end of the micromixer, and the correct incubation time required by the protocol is met.

3.1.2.1 Laminar flow

Figure 3.3 shows the laminar flow results for the first proposed device. As already mentioned, the flow rate at both inlets is set at 1 µL/min. The whole platform is subject to low velocity, ranging from 10^{-4} to 10^{-3} m/s, so assumption of laminar flow is reasonable. Focusing on the mixing unit, at the obstacles restriction the velocity increases.

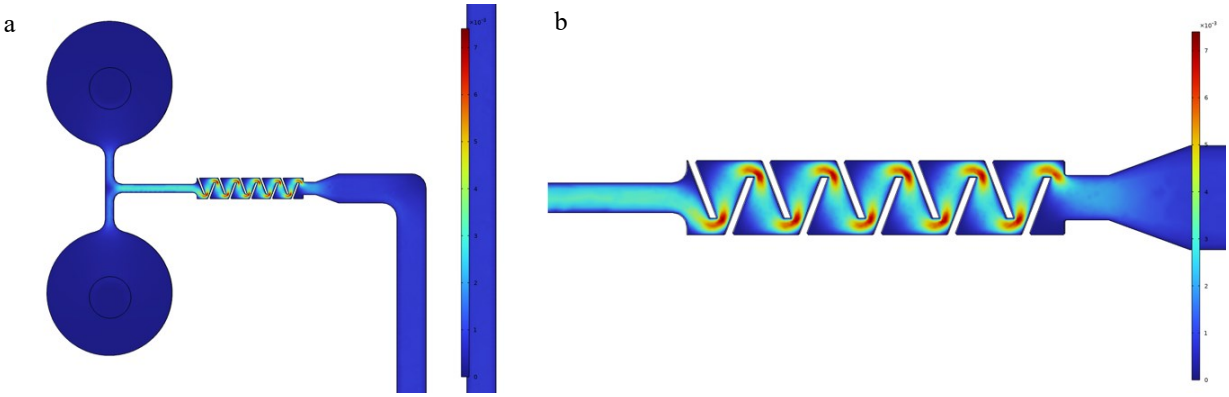

Figure 3.49 *COMSOL Multiphysics® laminar flow simulation of the first platform: a) T-type inlet channel; b) detail of the mixer.*

The 1-D plot confirms the laminar flow due to the parabolic nature of the velocity profile. The behavior is investigated at six different coordinates reported in Figure 3.4, both before and after the mixing unit.

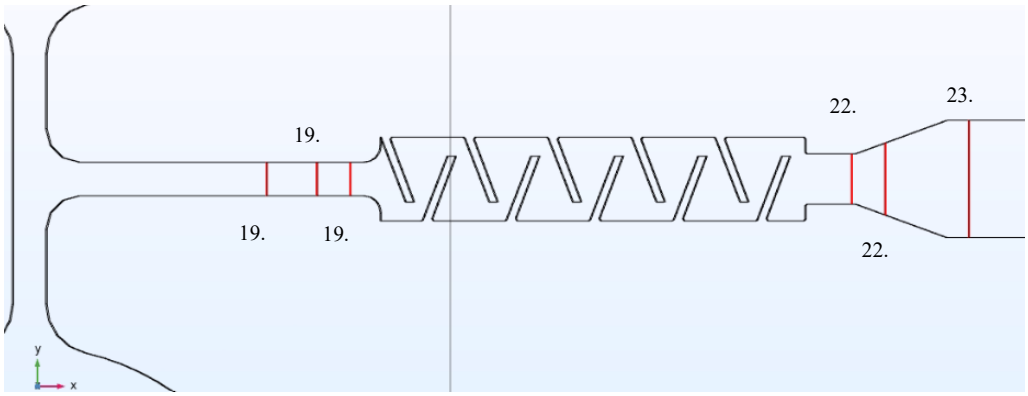

Figure 3.50 *COMSOL Multiphysics® coordinates before and after the mixing unit where the velocity behavior is investigated.*

Figure 3.5 shows the parabolic profile of velocity before the mixing unit, at coordinates 19.0, 19.3 and 19.5. Since no differences in the cross-sectional area are present, the curves are very similar, with an approximated maximum velocity of $3.2 \cdot 10^{-3}$ m/s.

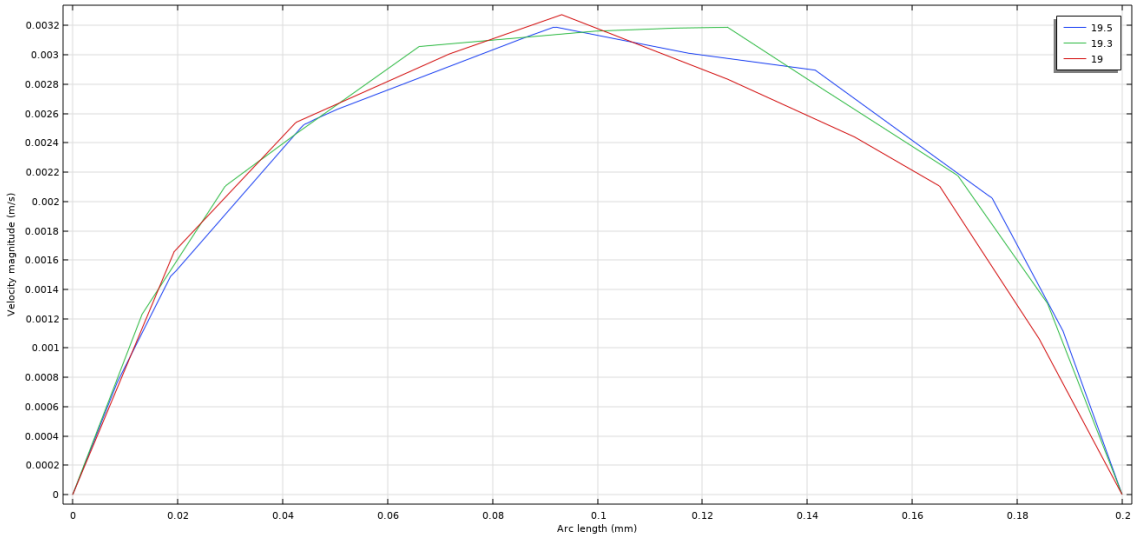

Figure 3.52 *Velocity profile of the first microfluidic platform before the mixing unit.*

Figure 3.6 shows velocity profiles after the micromixer. Some differences among the curves can be observed: at coordinate 23.2 (red) the maximum of the curve is lower than at coordinate 22.3 (blue) due to the widening of the cross-section (from 0.3 to 0.7 mm^2), which leads to a decrease in velocity. Indeed, the maxima are around $1.8 \cdot 10^{-3}$ and $0.7 \cdot 10^{-3}$ m/s, respectively.

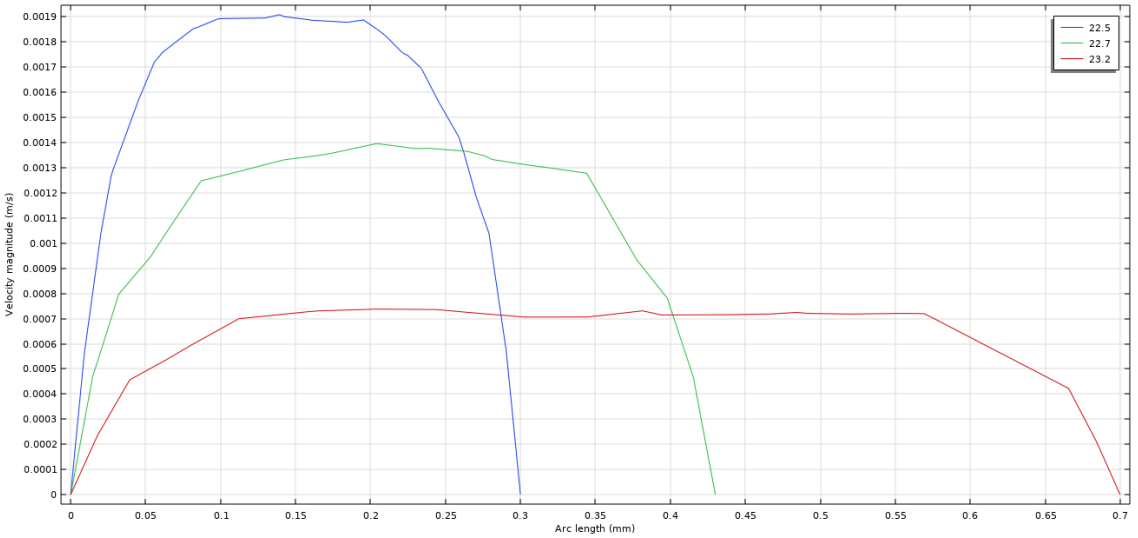

Figure 3.51 *Velocity profile of the first microfluidic platform after the mixing unit.*

Similar considerations can be applied to the revised platform. Figure 3.7 shows the velocity distribution for the entire platform. Again, the velocity is generally very low, increasing significantly only at the restrictions.

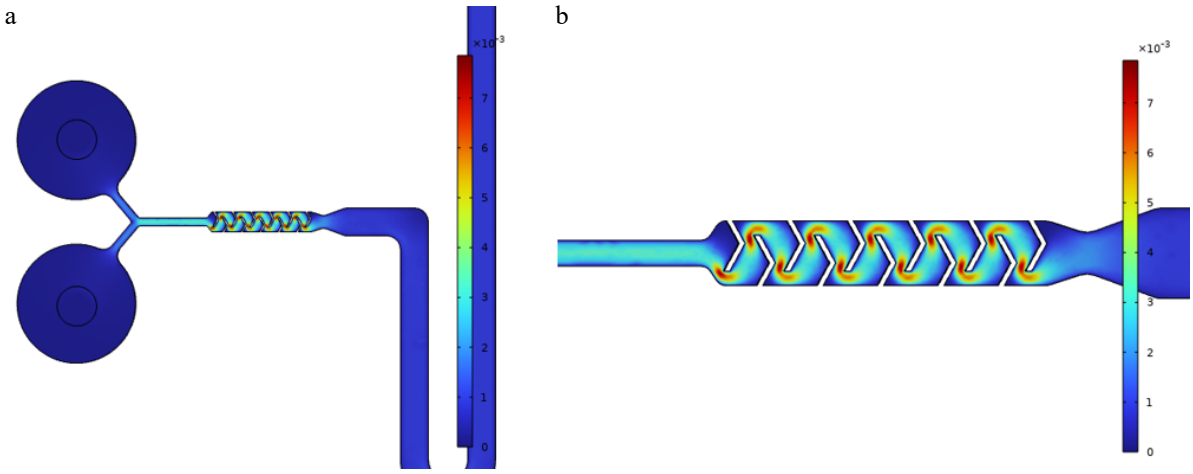

Figure 3.53 *COMSOL Multiphysics® laminar flow simulation of the second platform: a) Y-type inlet; b) detail of the mixer.*

As above, the behavior is investigated at six different coordinates reported in Figure 3.8, before and after the mixing unit.

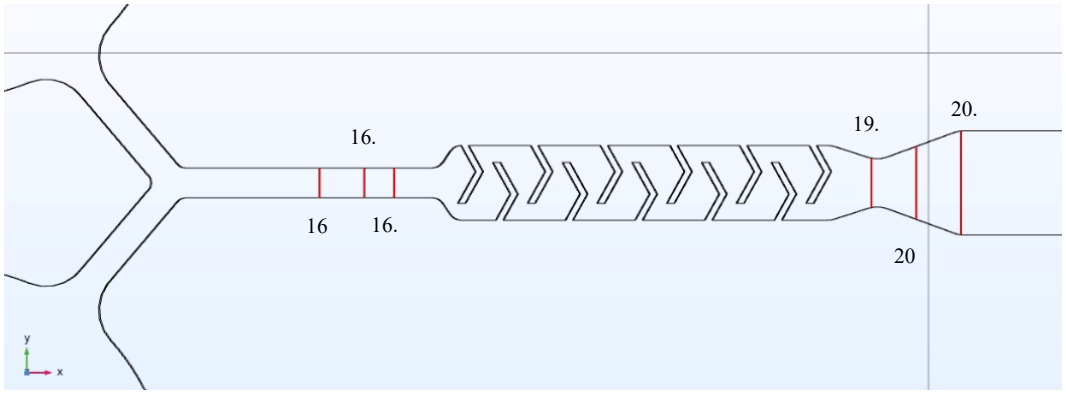

Figure 3.54 *COMSOL Multiphysics® coordinates before and after the mixing unit where the velocity behavior is investigated.*

In Figure 3.9 and Figure 3.10, the 1-D plots velocity profiles before and after the micromixer are reported. Since no changes are made to the geometry before the mixer, the maximum velocity of $3.2 \cdot 10^{-3}$ m/s does not change.

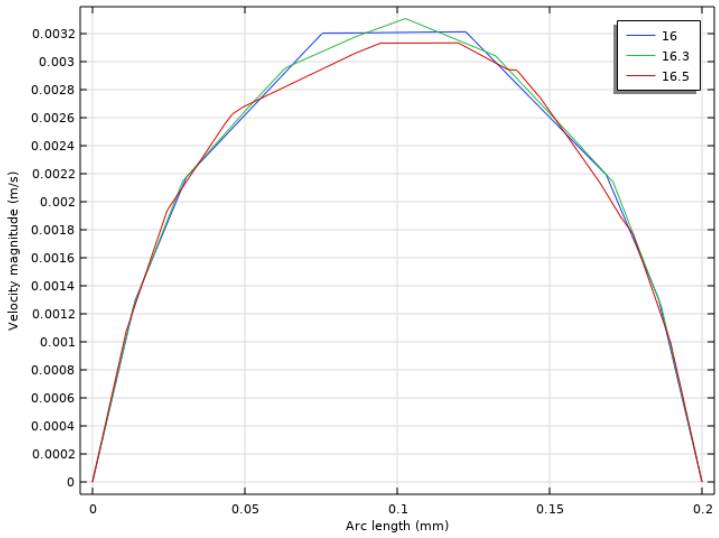

Figure 3.55 *Velocity profile of the second microfluidic platform before the mixing unit.*

On the other hand, a difference between the first and the revised platform can be observed when considering the velocities at the coordinates after the micromixer. The highest maximum velocity ($1.8 \cdot 10^{-3}$ m/s) is associated with coordinate 19.7, which is characterized by the smallest cross section (0.3 mm^2), while the lowest maximum velocity ($0.8 \cdot 10^{-3}$ m/s) corresponds to the coordinate where the cross-section widens (0.7 mm^2).

Overall, the parabolic behavior of velocities, characteristic of the laminar regime, confirm the working hypothesis of the platform.

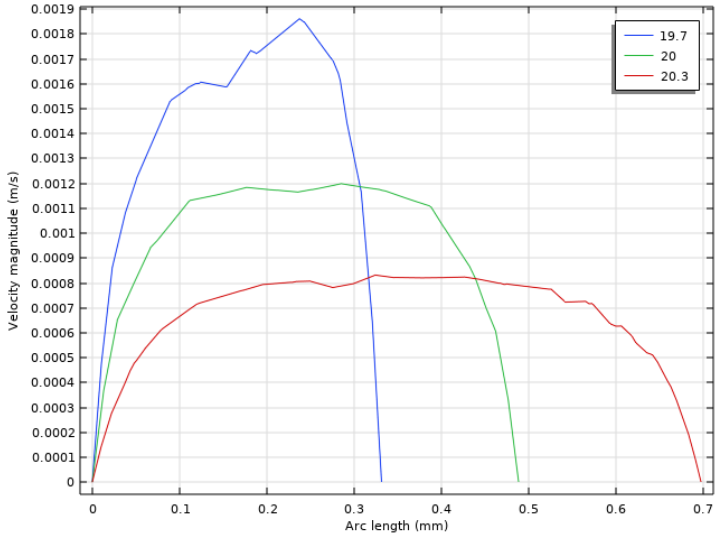

Figure 3.56 *Velocity profile of the second microfluidic platform after the mixing unit.*

Reynolds number can be calculated to further verify the nature of the regime. For this purpose, the average velocity of different planes is calculated with the help of a specific COMSOL Multiphysics® tool. To estimate the Re number, it is necessary to determine the equivalent diameter, since the channels do not have a circular cross-section. In addition, the solution is assumed to be water so that its physical properties density and viscosity, can be

used. In Equations 3.3 and 3.4 calculate the equivalent diameter before and after the mixing unit:

$$D_{eq,before} = \frac{4 \cdot 0.1 \cdot 0.2\ mm^2}{2 \cdot (0.1 + 0.2)\ mm} = 0.133\ mm \tag{3.28}$$

$$D_{eq,after} = \frac{4 \cdot 0.1 \cdot 0.7\ mm^2}{2 \cdot (0.1 + 0.7)\ mm} = 0.175\ mm \tag{3.29}$$

Table 3.1 shows the properties of water used to calculate the Re number:

Table 3.4 *Water properties: Density, Viscosity, Diffusion coefficient related to EVs.*

Substance	Density $[\boldsymbol{Kg/m^3}]$	Viscosity $[\boldsymbol{Pa \cdot s}]$	EVs-Diffusion coefficient $[\boldsymbol{m^2/s}]$
Water	1000	$8.9 \cdot 10^{-4}$	$3.44 \cdot 10^{-12}$

Finally, Re number can be estimated, according to the definition given in Equation 1.2. Table 3.2 shows the Re numbers and velocity values for both the first and the revised microfluidic chips, divided according to the position, before and after the mixing section.

Table 3.5 *Velocity and Re number results before and after the mixing section for both platforms.*

Platform	Velocity before mixing unit $[\boldsymbol{m/s}]$	Re before mixing unit	Velocity after mixing unit $[\boldsymbol{m/s}]$	Re after mixing unit
1	$1.5 \cdot 10^{-3}$	0.294	$0.5 \cdot 10^{-3}$	0.098
2	$1.5 \cdot 10^{-3}$	0.294	$0.44 \cdot 10^{-3}$	0.065

Since $Re \ll 2100$, both microfluidic devices work in a laminar regime.
Péclet number can also be calculated. Pe, defined in Equation 1.13, can be computed from the velocity inside the channel, the equivalent diameter, and the diffusion coefficient. Specifically, Pe is estimated before and after the mixing unit for the slower element of the two species present, that is EVs. Pe values, calculated according to Equation 1.5, are reported in Table 3.3.

Table 3.6 *Pe number results before and after the mixing unit for both platforms.*

Platform	Pe before mixing unit	Pe after mixing unit
1	57994	25436
2	57994	22383

Since Pe≫1, mass transport is mainly dominated by convection. Therefore, convection is included in the module of transport of dilute species.

3.1.2.2 Transport of diluted species

As mentioned above, in the module of transport of diluted species, the convective term is kept active. Figure 3.11 shows the concentration surface plot of both microfluidic devices, where red and blue colors refer to the pure species involved in the process, EVs and VP, and the green color indicates the mixing of fluids. It can be noted that the simulated fluids are perfectly mixed within the mixing unit.

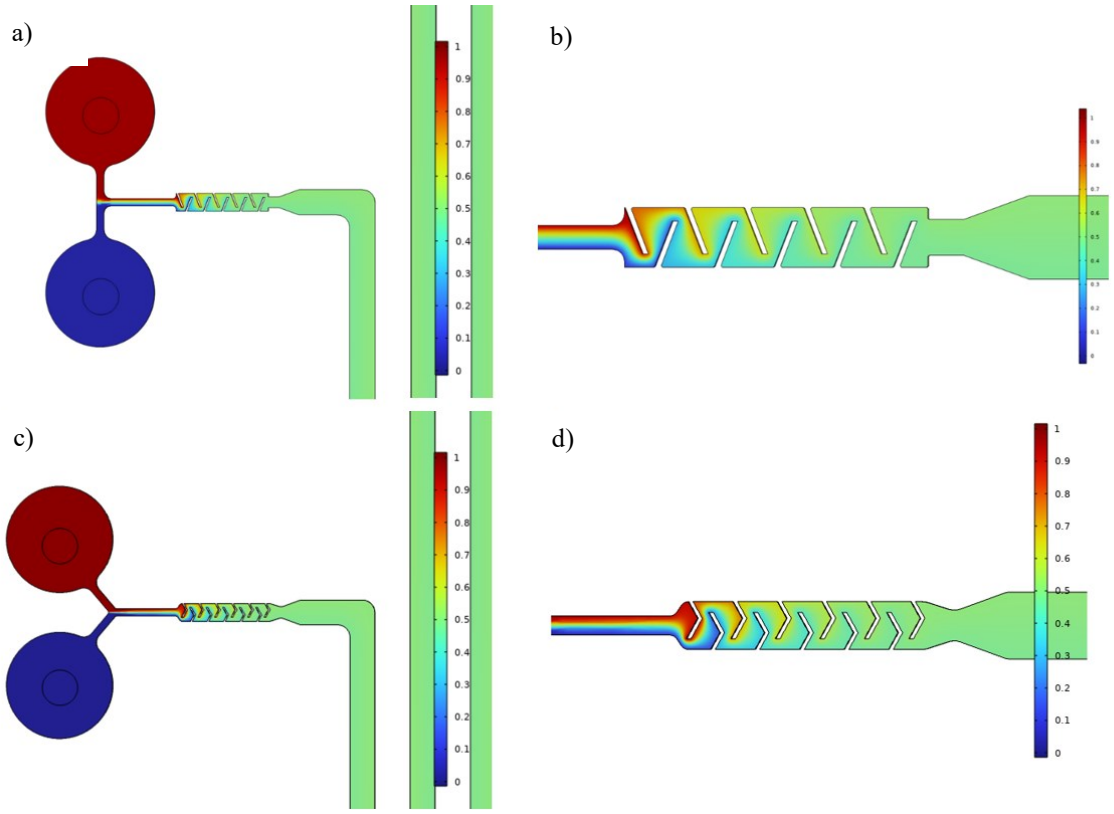

Figure 3.57 *COMSOL Multiphysics® concentration surface plots: a) first platform and b) first platform micromixer; c) second platform and d) second platform micromixer.*

Finally, the mixing index (η), defined according to Equation 3.5 proposed by Sarkar *et al.* (2014), is evaluated through a MATLAB® code, where COMSOL Multiphysics® retrieved concentration data are imported.

$$\eta = 1 - \sqrt{\frac{\gamma^2}{\gamma_{max}^2}} \tag{3.30}$$

The mixing indexes computed for the proposed platforms are 0.97 and 0.99 for the first and the second platform, respectively. The mixing indexes are very similar, which means that

there is no clear difference in the mixing performance between the two micromixers. However, the revised platform shows a slight improvement.

Finally, *time-dependent* simulations are performed to analyze the incubation time. Figure 3.12 shows the comparison of dilute species transport between the two microfluidic chips. The incubation time is set at 10 minutes, as required by the protocol.

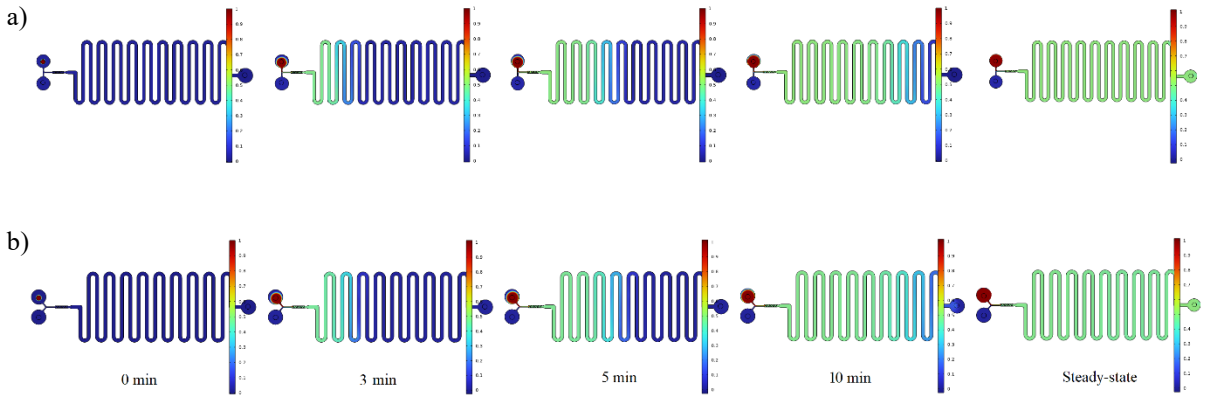

Figure 3.58 *Comparison of transport diluted species time-dependent COMSOL Multiphysics® simulations: a) first platform; b) second platform.*

3.1.3 Production of the master

The masters are produced in a clean room following the procedure explained in §2.1.3. As an example, the photomask and the master of the second platform are represented in Figure 3.13.

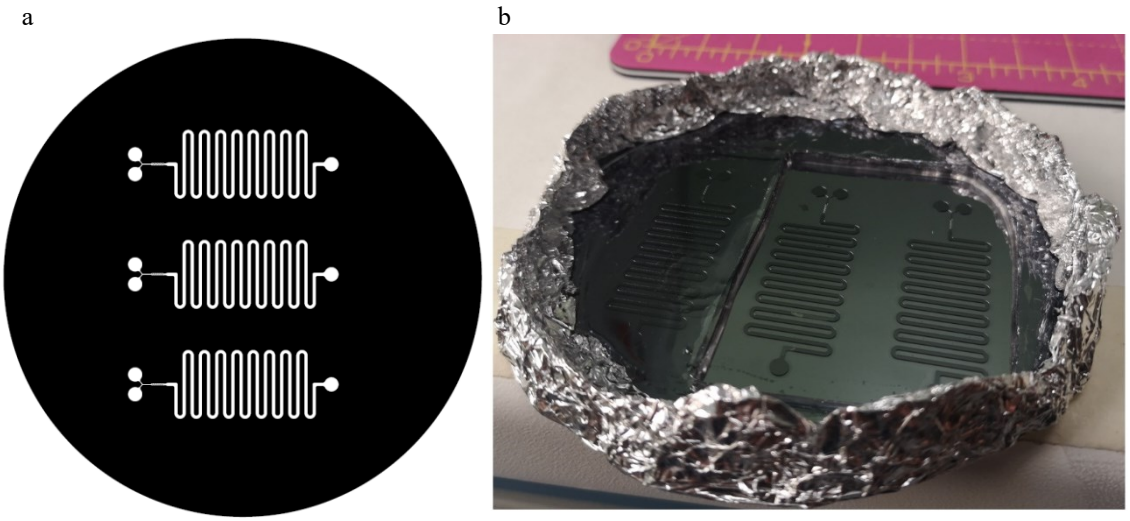

Figure 3.59 *Production of the master: a) photomask; b) master mold.*

3.1.4 Production of the platform

The platforms are then produced according to the protocol described in §2.1.4. Figure 3.14 and Figure 3.15 shows the layout of both PDMS platforms, highlighted with a green colorant.

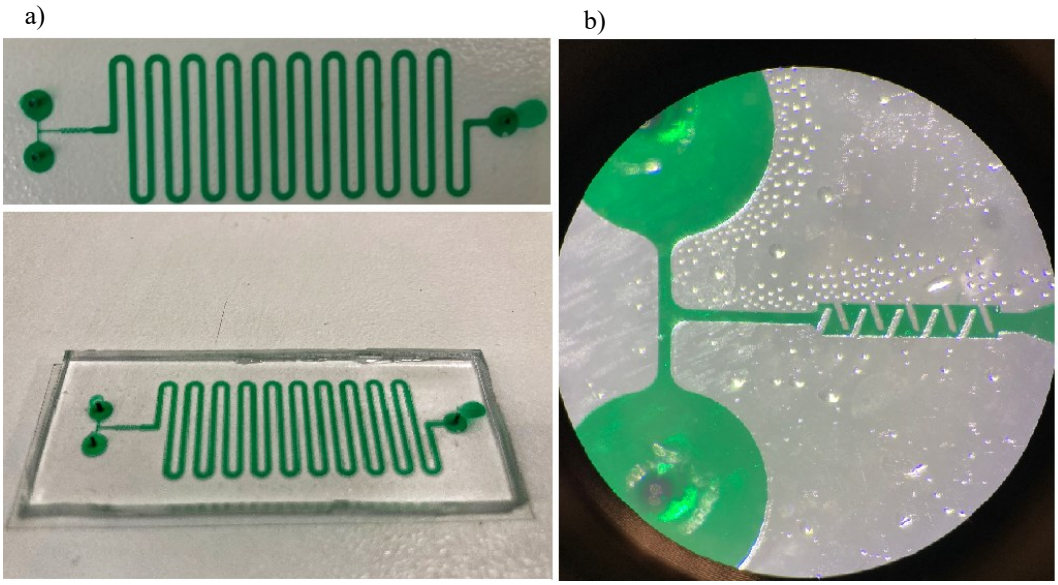

Figure 3.60 *First PDMS microfluidic device: a) entire platform; b) detail of the mixing unit, observed using a Stereomicroscope (Zeiss).*

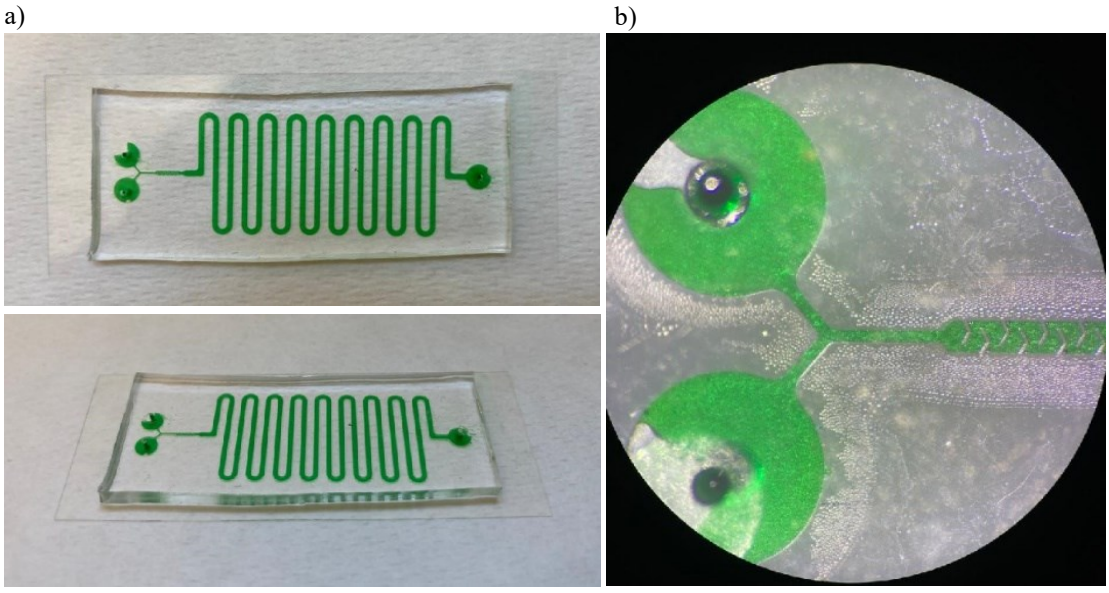

Figure 3.61 *Second PDMS microfluidic device: a) entire platform; b) detail of the mixing unit, observed using a Stereomicroscope (Zeiss).*

3.2 Platform validation

Platform validation is a crucial phase of the project as it allows comparing the computational work with the actual behavior of the device and, if necessary, modifying its structure to improve its performance. The results of fluid dynamic and biological validation are analyzed below.

3.2.1 Fluid dynamic validation

As explained in Chapter 2, the fluid dynamic validation is performed using both dextrans and food coloring.

Fluorescent isothiocyanate-dextrans are injected into the microfluidic system with the help of a micropipette. Figure 3.16 shows some representative details of the first device: the T-type inlet channel, the micromixer geometry, and the incubation coil can be appreciated. Notably, air bubbles tend to form at the ending section of the micromixer.

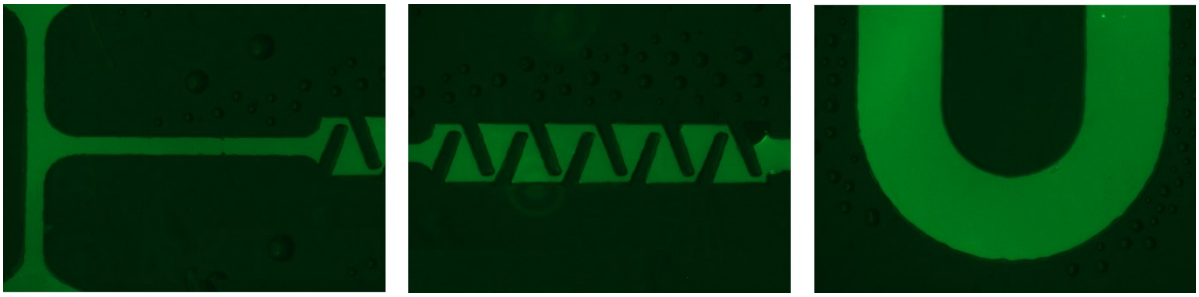

Figure 3.62 *Result of the validation experiment with fluorescent isothiocyanate-dextran on the irreversible configuration of the first microfluidic platform.*

Figure 3.17 shows the validation of the revised platform: the Y-type inlet channel, the micromixer, and a detail of the coil are visible. No air bubbles form at the micromixer.

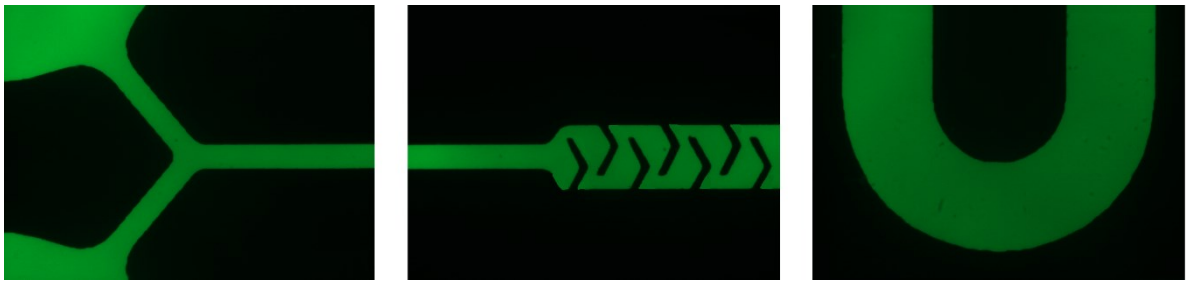

Figure 3.63 *Result of the validation experiment with fluorescent isothiocyanate-dextran on the irreversible configuration of the second microfluidic platform.*

Colored tracers are infused with the PHD Ultra pump (Harvard Apparatus). Figure 3.18 compares the microfluidic devices injected with yellow and blue dyes, with steady-state simulations, confirming that perfect mixing is achieved.

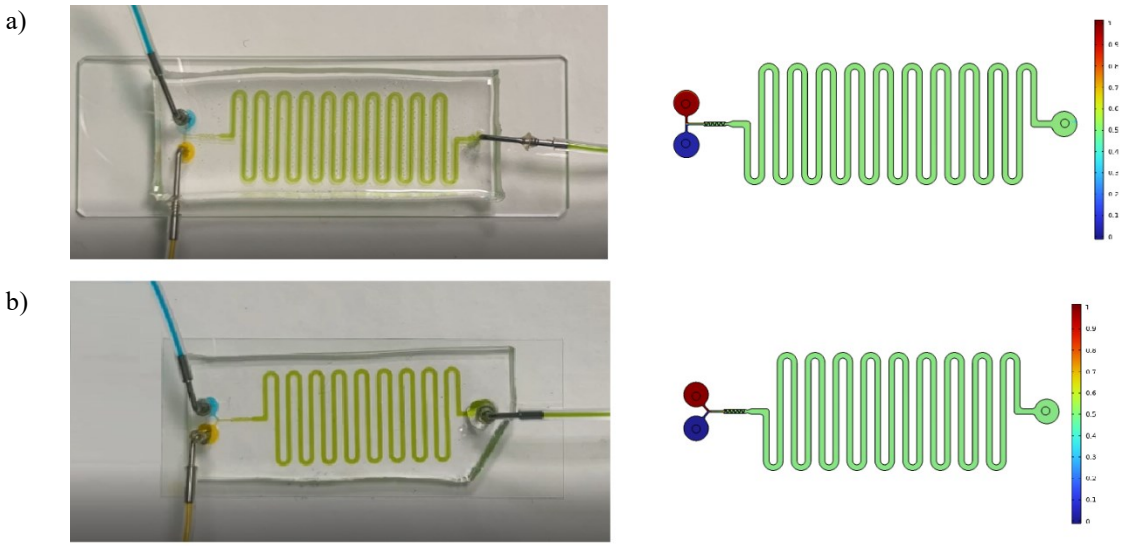

Figure 3.64 *Comparison between the fluid dynamic validation experiments and the COMSOL Multiphysics® steady-state simulations: a) first microfluidic system; b) second microfluidic system.*

Figure 3.19 reports the comparison between COMSOL Multiphysics® *time-dependent* simulation and the fluid dynamic validation for the first microfluidic device, demonstrating that perfect mixing and timing are obtained using the platform.

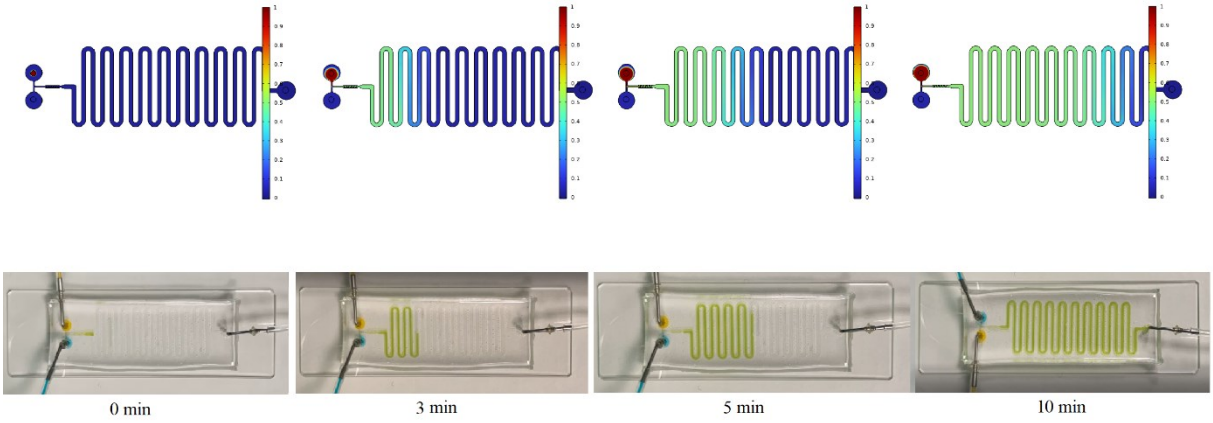

Figure 3.65 *First microfluidic platform: comparison between time-dependent simulation and fluid dynamic validation.*

Similarly, Figure 3.20 shows the same comparison for the second microfluidic chip. Here, the incubation timing seems even more accurate with respect to the previous design.

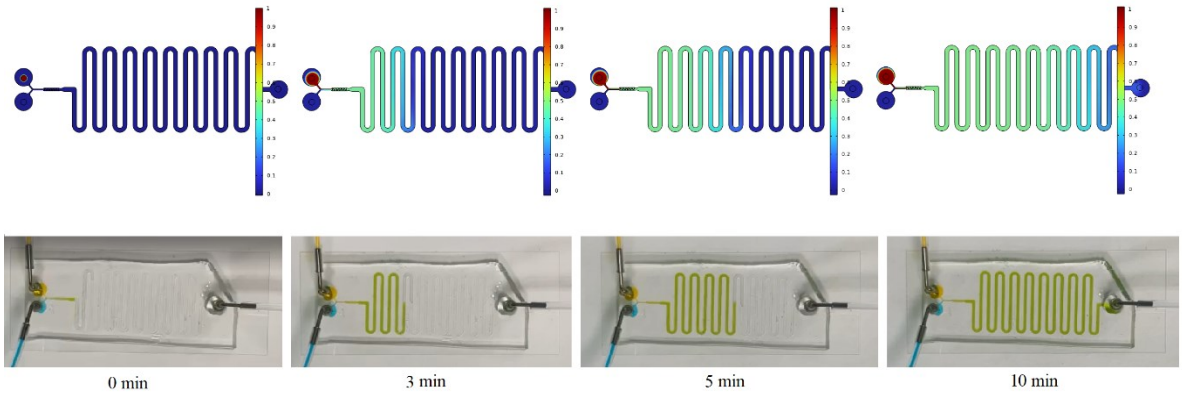

Figure 3.66 *Second microfluidic platform: comparison between time-dependent simulation and fluid dynamic validation.*

3.2.2 Biological validation

Biological validations are performed using the first platform. Biological validation of the second platform will be carried out in future studies. As already mentioned, about 10^9 EVs isolated from MSCs – and VP concentrated 1mM are used. The syringes with the EVs and VP are prepared and placed on the syringe pump, infusing with a flow rate of 1 µL/min. After approximately 10 minutes the mixed fluid comes out through the outlet, demonstrating that perfect mixing and timing are obtained using the platform. The mixed samples at the outlet are then processed through ultrafiltration to separate EVs from the excess of free VP.

3.3 Biological protocols

In this section, some considerations related to EVs isolation protocols, and EVs characterization are discussed.

3.3.1 EVs isolation

As explained in §2.3.3, EVs are extracted from MSCs. The standard isolation protocol consists of growing MSCs for 3 days in complete medium and 2 days in serum-free medium. Then, isolation is performed by ultrafiltration. Several isolation protocols were tested before optimization for our application. A first alternative protocol is to grow MSCs until 80% confluence is reached, usually achieved in 5 days. Subsequently, 2-days growth is performed in serum-free medium (Fuhrmann *et al.*, 2014). A second alternative consists of growing MSCs for 3 days in complete medium, and double isolation at 24 and 48 hours after replacement with serum-free medium (Patel *et al.*, 2017).

These procedures do not yield significant advantages in terms of the concentration of isolated EVs, as illustrated in Table 3.4. For this reason, the standard isolation protocol is used for all future experiments. In any case, it has been shown that no substantial changes in cell

morphology and viability appear when MSCs are cultured under serum-free conditions for up to 48 hours, as shown in Figure 3.21.

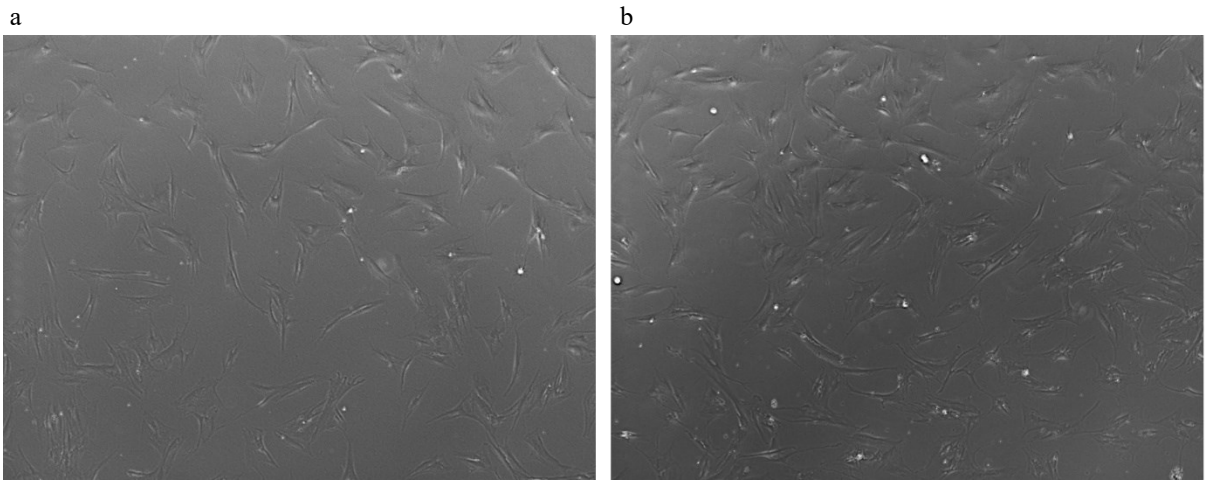

Figure 3.67 *Microscopy images of MSCs culture a) at the addition of serum-free medium b) after 48 hours.*

3.3.2 EVs characterization

EVs characterization is performed after every isolation, using BCA assay and NTA analysis, following the procedure described in §2.3.4. WB and TEM analyses are performed only for the first isolation to confirm the nature of the extracted vesicles.

3.3.2.1 BCA and NTA

Figure 3.22 illustrates the result of a representative NTA measurement. The plot represents the distribution of particle concentration versus size.

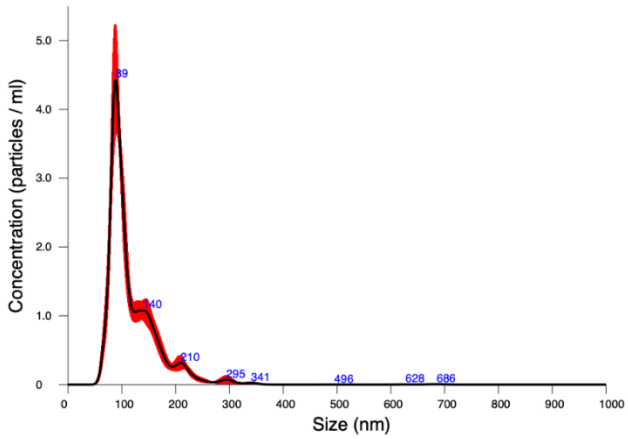

Figure 3.68 *Size distribution profile of EVs pre-loading analyzed by NTA.*

The results of both BCA and NTA for the first eight isolations performed are summarized in Table 3.4, where the distinction among the alternative protocols used is also specified.

Table 3.7 *EVs characterization before the drug-loading process: results of BCA assay and NTA.*

Sample #	Cell Number	BCA (µg/µL)	NTA (particles/mL)	Mean size (nm)	Protocol
1	$5.0 \cdot 10^5$	1.30	$1.78 \cdot 10^{10} \pm 1.78 \cdot 10^9$	129.9 ± 4.1	3+2 days standard
2	$4.8 \cdot 10^5$	1.30	$2.10 \cdot 10^{10} \pm 1.02 \cdot 10^9$	119.2 ± 2.2	3+2 days standard
3	$8.7 \cdot 10^5$	0.64	$2.45 \cdot 10^9 \pm 1.92 \cdot 10^8$	140.8 ± 6.3	5+2 days
4	$9.3 \cdot 10^5$	0.76	$3.62 \cdot 10^9 \pm 1.77 \cdot 10^7$	122.0 ± 3.9	5+2 days
5	$5.0 \cdot 10^5$	1.56	$3.16 \cdot 10^{10} \pm 2.27 \cdot 10^9$	149.4 ± 4.9	5+2 days
6	$8.0 \cdot 10^5$	0.72	$2.35 \cdot 10^9 \pm 9.8 \cdot 10^7$	124.4 ± 5.5	5+2 days
7.24	$5.1 \cdot 10^5$	0.11	$< 10^6$	–	3+2 days every 24 hours
7.48	$5.1 \cdot 10^5$	0.10	$< 10^6$	–	3+2 days every 24 hours

Overall, EVs size is around 131 nm, in line with what has been reported in the literature (30-1000 nm), whereas the protein content is between 0.76-1.76 µg/µL.

Notably, the results reported in Table 3.4 highlight that the greater the number of days in culture the lower the concentration of EVs. A clear decrease in EVs concentration is also detected by collecting the conditioned medium every 24 hours. Therefore, it is concluded that the best procedure for the EVs isolation is the standard protocol.

3.3.2.2 WB and TEM

As shown in Figure 3.23, WB detected the expression of EVs markers CD81, CD63 and the absence of negative marker Cytochrome C.

Figure 3.24 shows a representative image of purified EVs analyzed by TEM. As you can see from the Figure, the gold nanoparticle, associated with CD63 and shown as a black dot, is associated with the isolated EV.

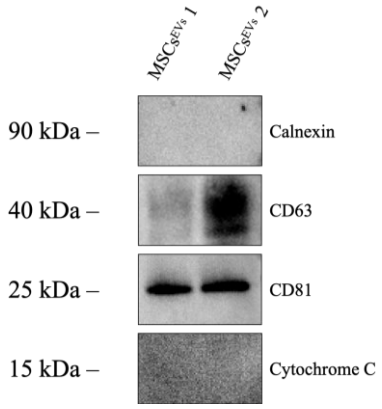

Figure 3.69 *Validation of EVs markers CD81, CD63 and negative marker Cytochrome C expression by WB analysis.*

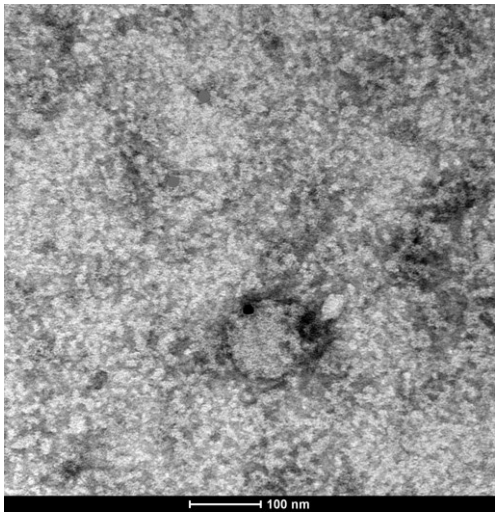

Figure 3.70 *Representative TEM image of a labeled EV.*

These data indicate that EVs are successfully isolated from MSCs.

3.4 Biological experiments

First, the results of the verification of the presence of VP within EVs are shown. In addition, a comparison of the loading efficiency between the standard off-chip protocol and the new on-chip protocol is presented. Finally, preliminary results on the internalization of VP-loaded EVs and therapeutic effects on an NB target cell line are illustrated.

3.4.1 NTA

NTA analysis is used to assess the concentration and size of VP-loaded EVs. As an example, Figure 3.25 compares the concentration and size distribution of EVs before and after the VP-loading process using Sample #5. The EVs analyzed before the loading process have a mean size of 149 nm and a particle concentration of $3.16 \cdot 10^{10} \pm 2.27 \cdot 10^{9}$ particles/mL, as already reported in Table 3.4. The same EVs loaded with VP have a mean size of 178 nm and a concentration of $1.65 \cdot 10^{8} \pm 7.10 \cdot 10^{6}$ particles/mL.
As expected, the average size of loaded particles is slightly larger, while the concentration is slightly lower due to the partial loss of vesicles during the experiment.

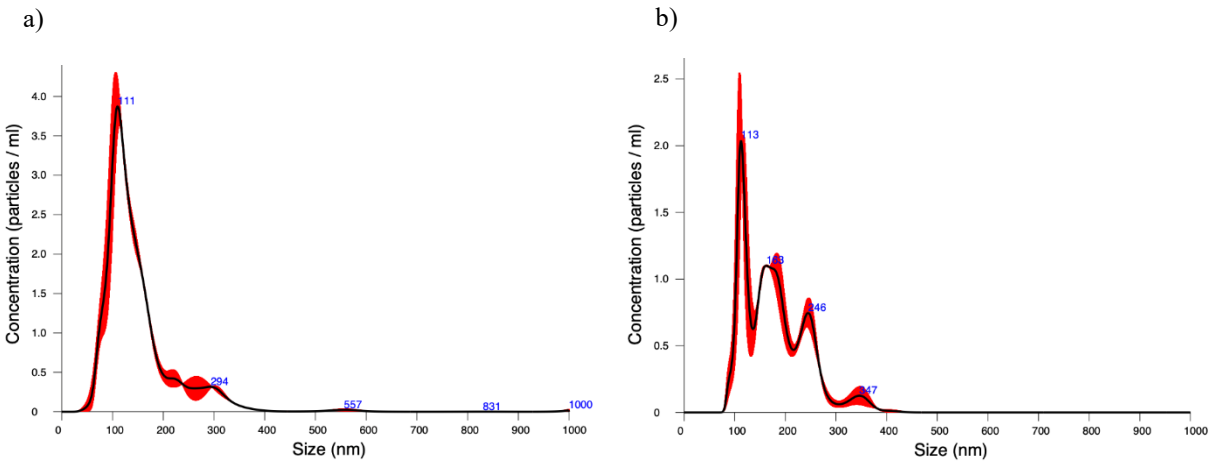

Figure 3.71 *Size distribution profile of a) pre-loading EVs and b) post-loading EVs analysed by NTA.*

3.4.2 Absorbance and Fluorescence

Considering spectral properties, VP-loaded EVs displayed similar absorption and fluorescent profiles compared to free VP, demonstrating the loading capability of the microfluidic system.

Figure 3.26 reports a representative absorbance spectra (450-800 nm) for both the free VP and VP-loaded EVs. Their overlapping absorption profiles show the presence of a peak at the 690 nm wavelength, confirming the presence of VPs within the EVs.

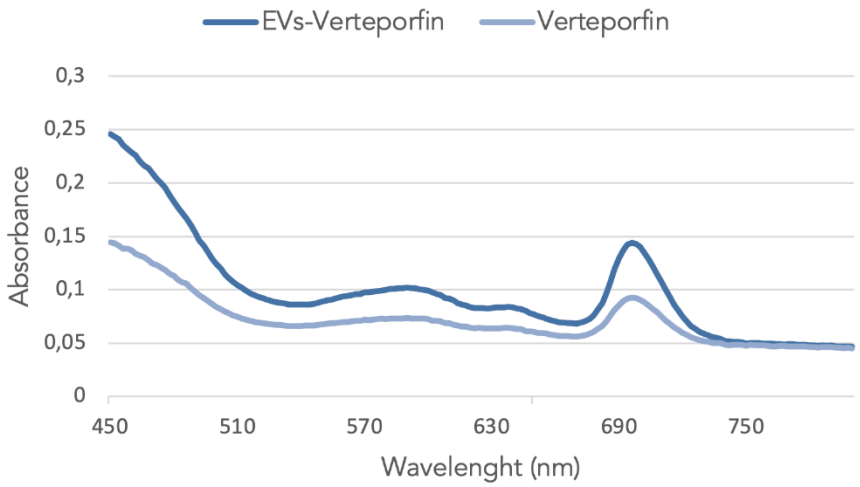

Figure 3.72 *Absorption spectra of 10μM free VP at (light blue) and VP-loaded EVs (dark blue). Measurements are performed using Tecan Spark multimode microplate reader.*

Figure 3.27 shows that the loading capability is also confirmed by comparable fluorescence emission signal intensity from VP and VP-loaded EVs after excitation at 420 nm.

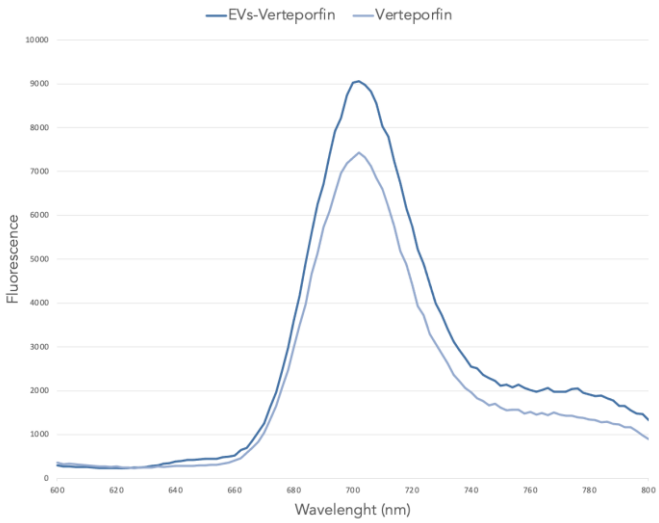

Figure 3.73 *Fluorescence spectra of 10μM free VP at (light blue) and VP-loaded EVs (dark blue). Measurements are performed using Tecan Spark multimode microplate reader.*

It is important to remember that absorbance analysis also makes it possible to determine the concentration of VP loaded within EVs. In fact, by constructing a calibration curve using known concentrations of VP, the concentration of the unknown sample can be estimated. Based on the calculated absorbance values, the calculation of *Loading* in terms of VP molecules per vesicle can be performed. The calculation is done through Equation 3.6:

$$Loading = \frac{VP\ concentration\ in\ the\ sample\ [\mu M]}{EVs\ concentration\ post-loading\ [\frac{vesicles}{L}]} \tag{3.31}$$

Results of the *Loading off-chip*, i.e., using the conventional protocol proposed by Fuhrmann *et al.* (2015), and *on-chip*, i. e. using microfluidics, are reported.

$$Loading_{on-chip} = 1.7 \cdot 10^8 \frac{molecules}{vesicles} \tag{3.32}$$

$$Loading_{off-chip} = 1.4 \cdot 10^7 \frac{molecules}{vesicles} \tag{3.33}$$

The Loading efficiency can be expressed as the ratio between the two:

$$Loading_{efficiency} = \frac{Loading_{on-chip}}{Loading_{off-chip}} \tag{3.34}$$

The comparison of the two protocols results in a loading performance 10-fold higher for the microfluidic approach than for the *off-chip* procedure.

$$Loading_{efficiency} = 10^1 \quad (3.35)$$

Therefore, these preliminary results demonstrate that microscale greatly improves the drug loading process.

3.4.3 Immunofluorescence

Immunofluorescence is performed to analyze SK-N-AS cells response to treatment with either free-VP or VP-loaded EVs, according to the protocol explained in §2.4.3.
First, cellular uptake of VP-loaded EVs in SK-N-AS is evaluated. Confocal microscopy shows that VP-loaded EVs (expressing red fluorescence signal) are mostly found in the cytoplasm of SK-N-AS cells, confirming their internalization in cells (Figure 3.29).

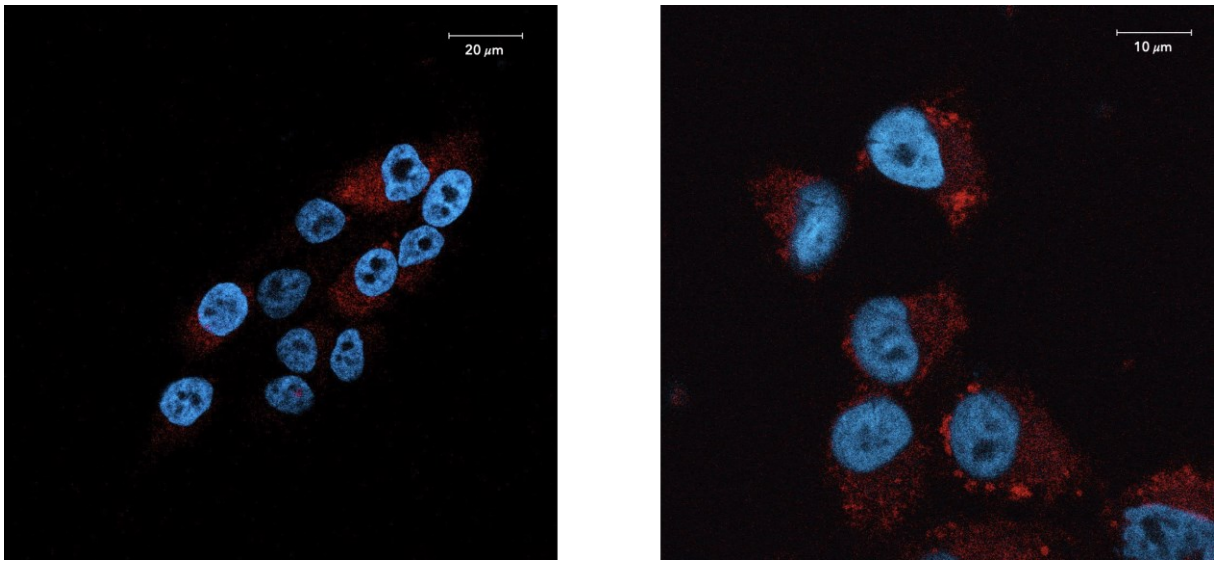

Figure 3.74 *Confocal microscopy images of SK-N-AS cells treated with 5 μM VP-loaded EVs for 24 h. VP is visualized in red, while nuclei are marked in blue with DAPI. Images are taken with the Zeiss LSM800 Airyscan Confocal microscopy.*

As already anticipated, VP is an inhibitor of the YAP/TAZ complex. Therefore, the difference in YAP gene expression in treated and untreated SK-N-AS cells is evaluated.
As can be seen from this preliminary result in Figure 3.30, YAP expression appears to be lower in treated than in control samples.

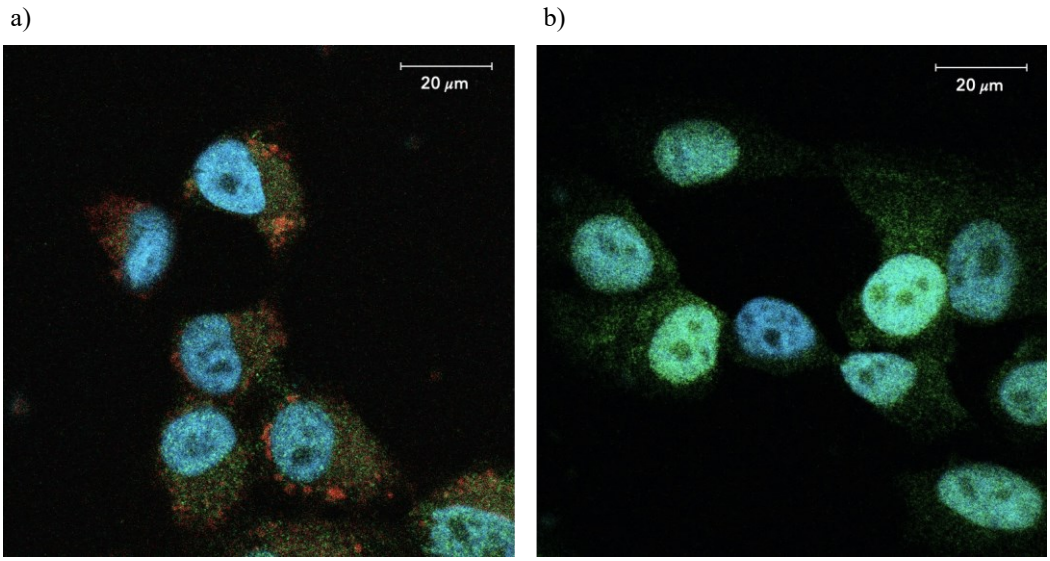

Figure 3.75 *Confocal microscopy images of NB cells. VP is visualized in red, while nuclei and YAP are marked respectively in blue with DAPI and in green with Alexa Fluor 488. a) Treated cells with VP-loaded EV b) Control.*

To quantify YAP signal and thus understand whether the difference between treated and control samples is statistically significant, image analysis is performed using ImageJ software. The data are displayed in a box plot (Figure 3.31) and a t-test analysis is performed to determine the statistical difference, using GraphPad Software. The expression of YAP is significantly different in the two samples, with a p-value<0.00001 (****), preliminarily confirming the inhibitory activity of VP on YAP.

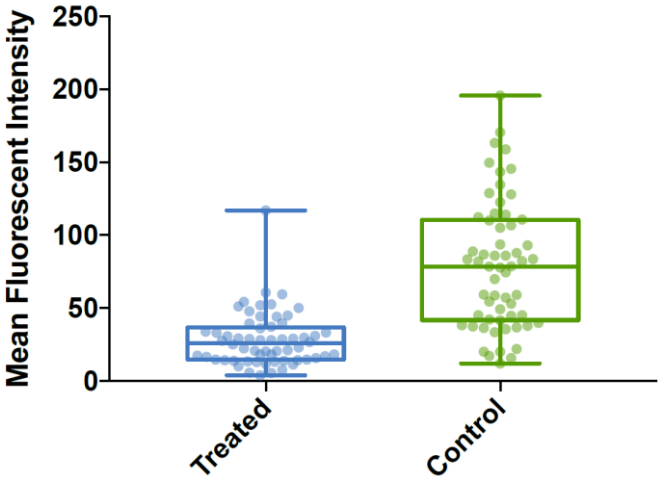

Figure 3.76 *Box Plot of MFI signal for both treated and control samples.*

3.4.4 MTT assay

MTT assay is carried out following the protocol described in §2.4.4. SK-N-AS cells are treated with either VP-loaded EVs or with free-VP. Figure 3.32 shows the percent cell viability as a function of the logarithmic concentration of VP-loaded EVs. A decrease in cell viability is observed with increasing VP concentration.
The IC_{50} at 48 h for VP-loaded EVs, calculated using GraphPad Software, is 0.85 μM.

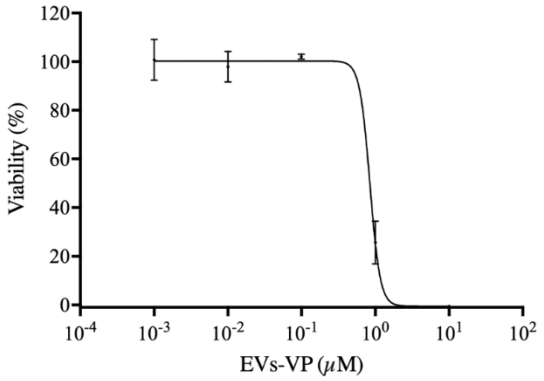

Figure 3.77 *Cell viability of SK-N-AS cells is measured by MTT test after 48 h of incubation with VP-loaded EVs. The data are plotted as a logarithmic function of the concentration of VP-loaded EVs.*

Figure 3.33 shows the results for the MTT assay performed after VP treatment.
Confirming the study of Fusco *et al.* (2021), the treatment with free-VP reduces cell viability, and the calculated IC_{50} is 1.33 μM.

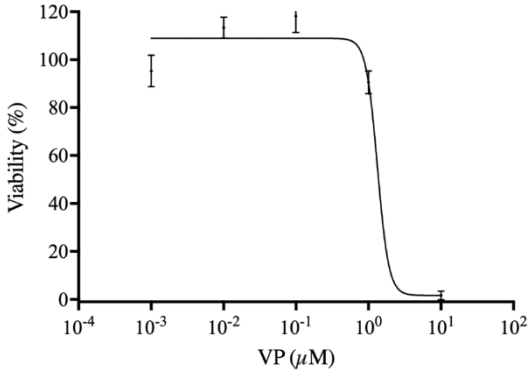

Figure 3.78 *Cell viability of SK-N-AS cells is measured by MTT test after 48 h of incubation with VP. The data are plotted as a logarithmic function of the concentration of VP.*

In conclusion, these preliminary results suggest that the concentration of VP required to achieve 50% cell death is higher when free-VP treatment is using the only-VP method, implying a more targeted effect of the VP-loaded EVs.

Conclusions

The aim of the project is the design and development of a microfluidic device for generating VP-loaded EVs.

MSCs are used as cell sources of EVs for therapeutic purposes. Once isolated using ultrafiltration, MSC-derived EVs are characterized by multiple and complementary techniques. These data indicated that EVs are successfully isolated from MSCs.

VP is used as it is a naturally fluorescent photosensitizer that represents a potential approach for NB therapy.

Two platforms are proposed and designed using AutoCAD® so that both a perfect mixing between MSCs-derived EVs and VP occurs within the mixing unit and the desired incubation time, set at 10 minutes, is achieved. The difference between the two platforms lies mainly in the mixing unit, which is redesigned to achieve perfect mixing without air bubble formation. The length of the delay lines in the incubation unit is modified accordingly.

The platforms are then modeled, performing computational fluid dynamics simulations through COMSOL Multiphysics®: the simulated fluids are perfectly mixed within the mixing unit, also demonstrated by the mixing index that is calculated to assess the mixing performance.

The master molds are fabricated with photolithography, and polydimethylsiloxane (PDMS) microfluidic chips are obtained with replica molding processes. Plasma treatment is used to form an irreversible hydraulic seal of the microfluidic platform to a glass support.

The platforms in this configuration are used to perform both fluid dynamic validations, using different tracers, and biological validations, using MSCs-derived EVs and VP.

Fluid dynamic validation confirms not only the correct production of the PDMS replica and the hydraulic seal of the platform, but also that perfect mixing and incubation times are obtained. Biological validation is conducted using 10^9 MSCs-derived EVs and 1mM VP. Considering spectral properties, VP-loaded EVs display similar absorption and fluorescence profiles compared to free VP, confirming that highly efficient loading of VP into EVs is obtained, calculated to be an order of magnitude higher than standard protocols described in the literature.

Preliminary biological experiments show that VP-loaded EVs could be able to produce a therapeutic effect on a target NB cell line. Specifically, IF analysis confirmed that VP-loaded EVs internalized into cells modify YAP expression, corroborating what has been reported in the literature. Finally, MTT assay is employed to extrapolate the IC_{50}, which is used in pharmacology to measure the potency of a given agent.

Although very promising, further experiments are needed to confirm the preliminary results obtained.

In conclusion, the platform was designed, modeled, and produced and its fluid dynamic and biological validation demonstrated its proper functioning.

The next few steps will be aimed at verifying EVs ability to retain the drug under *in vivo* simulating conditions. To that end, a microfluidic-based *organ-on-a-chip* that incorporates the primary tumor, metastatic tissue targets, and microfluidic perfusion could be used for testing the potential of the engineered EVs to deliver the drugs to the target cells of interest. Thus, as a versatile tool, microfluidic technology could help to fully unlock the potential of EVs.

Nomenclature

Roman symbols

c	=	Concentration [mol/m3]
Ca	=	Capillary number [dimensionless]
D	=	Diameter [m]
D_{eq}	=	Equivalent diameter [m]
D_i	=	Diffusion coefficient of the species i [m2/s]
E_{exp}	=	Exposure energy
g	=	Acceleration gravity [m/s2]
h	=	Height of the channel [m]
J_i	=	Diffusive flux of the species i [mol/s]
k_B	=	Boltzmann constant [J/K]
l	=	Length of the channel [m]
P	=	Semiperimeter [m]
Pe	=	Péclet number [dimensionless]
r	=	Radius [m]
Re	=	Reynolds number [dimensionless]
R_i	=	Reaction term
S	=	Section of the channel [m2]
T	=	Temperature [K]
t_{exp}	=	Exposure time
$\dot{V}$	=	Volumetric flowrate [m^3/s]
v	=	Velocity [m/s]
w	=	Width of the channel [m]
ΔP	=	Pressure drops [Pa]
ΔP^*	=	Dimensionless pressure drops [dimensionless]

Greek symbols

μ	=	Dinamic viscosity [Pa·s]
γ	=	Surface tension [N]
γ	=	Variance
η	=	Mobility of the particle [kg/s]
η	=	Mixing index [dimensionless]
ϑ	=	Delay time [time]
ρ	=	Density [kg/m3]

v	=	Cinematic viscosity [m2/s]

Acronyms

AEs	=	Algebraic Equations system
BCA	=	Bicinchoninic Acid Protein Assay
BSA	=	Bovine Serum Albumin
CFD	=	Computational fluid dynamic
CM	=	Conditioned Medium
DAEs	=	Differential and Algebraic Equations system
DMSO	=	Dimethyl sulfoxide
DAPI	=	Diamidino-2-phenylindole
EVs	=	Extracellular vesicles
FBS	=	Fetal Bovine Serum
HB	=	Hard Bake
IF	=	Immunofluorescence
MP	=	Mixing performance [dimensionless]
MSCs	=	Mesenchymal stem cells
NB	=	Neuroblastoma
NTA	=	Nanoparticle Tracking Analysis
PBS	=	Phosphate Buffered Saline
PEB	=	Post exposure bake
PFA	=	Paraformaldehyde
P/S	=	Penicillin/Streptomycin
PDMS	=	Polydimethylsiloxane
SB	=	Soft Bake
TEM	=	Transmission Electron Microscopy
VP	=	Verteporfin
WB	=	Western Blot

References

Bebelman, M. P., Smit, M. J., Pegtel, D. M., & Baglio, S. R. (2018). Biogenesis and function of extracellular vesicles in cancer. In *Pharmacology and Therapeutics* (Vol. 188, pp. 1–11). Elsevier Inc. https://doi.org/10.1016/j.pharmthera.2018.02.013

Beebe, D. J., Mensing, G. A., & Walker, G. M. (2002). Physics and Applications of Microfluidics in Biology. *Annual Review of Biomedical Engineering*, *4*(1), 261–286. https://doi.org/10.1146/annurev.bioeng.4.112601.125916

Breslauer, D. N., Lee, P. J., & Lee, L. P. (2006). Microfluidics-based systems biology. *Molecular BioSystems*, *2*(2), 97–112. https://doi.org/10.1039/b515632g

Davidoff, A. M., Fernandez-Pineda, I., Santana, V. M., & Shochat, S. J. (2012). The role of neoadjuvant chemotherapy in children with malignant solid tumors. *Seminars in Pediatric Surgery*, *21*(1), 88–99. https://doi.org/10.1053/j.sempedsurg.2011.10.010

Dittrich, P. S., & Manz, A. (2006). Lab-on-a-chip: Microfluidics in drug discovery. *Nature Reviews Drug Discovery*, *5*(3), 210–218. https://doi.org/10.1038/nrd1985

Eleveld, T. F., Oldridge, D. A., Bernard, V., Koster, J., Daage, L. C., Diskin, S. J., Schild, L., Bentahar, N. B., Bellini, A., Chicard, M., Lapouble, E., Combaret, V., Legoix-Né, P., Michon, J., Pugh, T. J., Hart, L. S., Rader, J., Attiyeh, E. F., Wei, J. S., … Maris, J. M. (2015). Relapsed neuroblastomas show frequent RAS-MAPK pathway mutations. *Nature Genetics*, *47*(8), 864–871. https://doi.org/10.1038/ng.3333

Fang, Y., Ye, Y., Shen, R., Zhu, P., Guo, R., Hu, Y., & Wu, L. (2012). Mixing enhancement by simple periodic geometric features in microchannels. *Chemical Engineering Journal*, *187*, 306–310. https://doi.org/10.1016/j.cej.2012.01.130

Frenz, L., Blank, K., Brouzes, E., & Griffiths, A. D. (2009). Reliable microfluidic on-chip incubation of droplets in delay-lines. *Lab on a Chip*, *9*(10), 1344–1348. https://doi.org/10.1039/b816049j

Fu, X., Liu, S., Ruan, X., & Yang, H. (2006). Research on staggered oriented ridges static micromixers. *Sensors and Actuators, B: Chemical*, *114*(2), 618–624. https://doi.org/10.1016/j.snb.2005.06.023

Fuhrmann, G., Serio, A., Mazo, M., Nair, R., & Stevens, M. M. (2015). Active loading into extracellular vesicles significantly improves the cellular uptake and photodynamic effect of porphyrins. *Journal of Controlled Release*, *205*, 35–44. https://doi.org/10.1016/j.jconrel.2014.11.029

Fusco, P., Mattiuzzo, E., Frasson, C., Viola, G., Cimetta, E., Esposito, M. R., & Tonini, G. P. (2021). Verteporfin induces apoptosis and reduces the stem cell-like properties in Neuroblastoma tumour-initiating cells through inhibition of the YAP/TAZ pathway. *European Journal of Pharmacology*, *893*. https://doi.org/10.1016/j.ejphar.2020.173829

Gao, D., Liu, H., Jiang, Y., Lin, J. M., Gao, D., Liu, H., & Jiang, Y. (2012). Recent developments in microfluidic devices for in vitro cell culture for cell-biology research. In *TrAC - Trends in Analytical Chemistry* (Vol. 35, pp. 150–164). https://doi.org/10.1016/j.trac.2012.02.008

Giebel, B., Kordelas, L., & Börger, V. (2017). Clinical potential of mesenchymal stem/stromal cell-derived extracellular vesicles. In *Stem Cell Investigation* (Vol. 4, Issue 10). AME Publishing Company. https://doi.org/10.21037/sci.2017.09.06

Haeberle, S., & Zengerle, R. (2007). Microfluidic platforms for lab-on-a-chip applications. *Lab on a Chip*, *7*(9), 1094–1110. https://doi.org/10.1039/b706364b

Jonkman, J., Brown, C. M., Wright, G. D., Anderson, K. I., & North, A. J. (2020). Guidance for quantitative confocal microscopy. *Nature Protocols*. https://doi.org/10.1038/s41596-020-0307-7

Kim, L., Toh, Y. C., Voldman, J., & Yu, H. (2007). A practical guide to microfluidic perfusion culture of adherent mammalian cells. *Lab on a Chip*, *7*(6), 681–694. https://doi.org/10.1039/b704602b

Kosaka, N., Yoshioka, Y., Tominaga, N., Hagiwara, K., Katsuda, T., & Ochiya, T. (2014). Dark side of the exosome: the role of the exosome in cancer metastasis and targeting the exosome as a strategy for cancer therapy. *Future Oncology*, *10*(4), 671–681. https://doi.org/10.2217/fon.13.222

Kuncová-Kallio, J., & Kallio, P. J. (2006). PDMS and its suitability for analytical microfluidic devices. *Annual International Conference of the IEEE Engineering in Medicine and Biology - Proceedings*, 2486–2489. https://doi.org/10.1109/IEMBS.2006.260465

Lee, C. Y., Wang, W. T., Liu, C. C., & Fu, L. M. (2016). Passive mixers in microfluidic systems: A review. In *Chemical Engineering Journal* (Vol. 288, pp. 146–160). Elsevier. https://doi.org/10.1016/j.cej.2015.10.122

Luksch, R., Castellani, M. R., Collini, P., de Bernardi, B., Conte, M., Gambini, C., Gandola, L., Garaventa, A., Biasoni, D., Podda, M., Sementa, A. R., Gatta, G., & Tonini, G. P. (2016). Neuroblastoma (Peripheral neuroblastic tumours). In *Critical Reviews in Oncology/Hematology* (Vol. 107, pp. 163–181). Elsevier Ireland Ltd. https://doi.org/10.1016/j.critrevonc.2016.10.001

Mahbubul H. Shihan, Samuel G. Novo, Sylvain J. Le Marchand, Yan Wang, Melinda K. Duncan, & FARVO Professor. (2021). *A simple method for quantitating confocal fluorescent images*.

Maris, J. M. (2010). Recent advances in neuroblastoma. *New England Journal of Medicine*, *362*(23), 2202. https://doi.org/10.1056/nejmra0804577

Möller, A., & Lobb, R. J. (2020). The evolving translational potential of small extracellular vesicles in cancer. In *Nature Reviews Cancer* (Vol. 20, Issue 12, pp. 697–709). Nature Research. https://doi.org/10.1038/s41568-020-00299-w

Niculescu, A. G., Chircov, C., Bîrcă, A. C., & Grumezescu, A. M. (2021). Fabrication and applications of microfluidic devices: A review. In *International Journal of Molecular Sciences* (Vol. 22, Issue 4, pp. 1–26). MDPI AG. https://doi.org/10.3390/ijms22042011

Patel, D. B., Gray, K. M., Santharam, Y., Lamichhane, T. N., Stroka, K. M., & Jay, S. M. (2017). Impact of cell culture parameters on production and vascularization bioactivity of mesenchymal stem cell-derived extracellular vesicles. *Bioengineering & Translational Medicine*, *2*(2), 170–179. https://doi.org/10.1002/btm2.10065

Peinado, H., Alečković, M., Lavotshkin, S., Matei, I., Costa-Silva, B., Moreno-Bueno, G., Hergueta-Redondo, M., Williams, C., García-Santos, G., Ghajar, C. M., Nitadori-Hoshino, A., Hoffman, C., Badal, K., Garcia, B. A., Callahan, M. K., Yuan, J., Martins, V. R., Skog, J., Kaplan, R. N., … Lyden, D. (2012). Melanoma exosomes educate bone marrow progenitor cells toward a pro-metastatic phenotype through MET. *Nature Medicine*, *18*(6), 883–891. https://doi.org/10.1038/nm.2753

Perry's Chemical Engineers' Handbook. (2008).

Sarkar, S., Singh, K. K., Shankar, V., & Shenoy, K. T. (2014). Numerical simulation of mixing at 1-1 and 1-2 microfluidic junctions. In *Chemical Engineering and Processing: Process Intensification* (Vol. 85, pp. 227–240). https://doi.org/10.1016/j.cep.2014.08.010

Schramm, A., Köster, J., Assenov, Y., Althoff, K., Peifer, M., Mahlow, E., Odersky, A., Beisser, D., Ernst, C., Henssen, A. G., Stephan, H., Schröder, C., Heukamp, L., Engesser, A., Kahlert, Y., Theissen, J., Hero, B., Roels, F., Altmüller, J., … Schulte, J. H. (2015). Mutational dynamics between primary and relapse neuroblastomas. *Nature Genetics*, *47*(8), 872–877. https://doi.org/10.1038/ng.3349

Squires, T. M., & Quake, S. R. (2005). Microfluidics: Fluid physics at the nanoliter scSquires, T. M., & Quake, S. R. (2005). Microfluidics: Fluid physics at the nanoliter scale. Reviews of Modern Physics, 77(3), 977–1026.ale. *Reviews of Modern Physics*, *77*(3), 977–1026.

Tripathi, E., Patowari, P. K., & Pati, S. (2021). Numerical investigation of mixing performance in spiral micromixers based on Dean flows and chaotic advection. *Chemical Engineering and Processing - Process Intensification*, *169*(July), 108609. https://doi.org/10.1016/j.cep.2021.108609

Udaya Kumar, A., Sai Ganesh, D., Vamsi Krishna, T., Sashank, B., & Satyanarayana, T. (2021). Modeling and investigation on mixing characteristics of T & Y-shaped micromixers for microfluidic devices. *Materials Today: Proceedings*, *xxxx*, 1–5. https://doi.org/10.1016/j.matpr.2021.11.474

Walker, S., Busatto, S., Pham, A., Tian, M., Suh, A., Carson, K., Quintero, A., Lafrence, M., Malik, H., Santana, M. X., & Wolfram, J. (2019). *Theranostics Extracellular vesicle-based drug delivery systems for cancer treatment*. *9*(26). https://doi.org/10.7150/thno.37097

Weibel, D. B., DiLuzio, W. R., & Whitesides, G. M. (2007). Microfabrication meets microbiology. *Nature Reviews Microbiology*, *5*(3), 209–218. https://doi.org/10.1038/nrmicro1616

Xu, R., Rai, A., Chen, M., Suwakulsiri, W., Greening, D. W., & Simpson, R. J. (2018). Extracellular vesicles in cancer — implications for future improvements in cancer care. In *Nature Reviews Clinical Oncology* (Vol. 15, Issue 10, pp. 617–638). Nature Publishing Group. https://doi.org/10.1038/s41571-018-0036-9

Yuan, S., Jiang, B., Peng, T., Zhou, M., & Drummer, D. (2022). Investigation of efficient mixing enhancement in planar micromixers with short mixing length. *Chemical Engineering and Processing - Process Intensification*, *171*(September 2021), 108747. https://doi.org/10.1016/j.cep.2021.108747

Zhou, J., Ellis, A. V., & Voelcker, N. H. (2010). Recent developments in PDMS surface modification for microfluidic devices. In *Electrophoresis* (Vol. 31, Issue 1, pp. 2–16). https://doi.org/10.1002/elps.200900475

Zhu, Q., Heon, M., Zhao, Z., & He, M. (2018). Microfluidic Engineering of Exosomes : Editing Cellular Messages for Precision Lab on a Chip Microfluidic engineering of exosomes : editing cellular messages for precision therapeutics. *Lab on a Chip*, *May*. https://doi.org/10.1039/C8LC00246K

Websites:

https://plasmatreatment.co.uk/ (Accessed: 20th August 2022)

https://www.sigmaaldrich.com/ (Accessed: 20th August 2022)

http://harrickplasma.com/ (Accessed: 22th August 2022)

https://www.thermofisher.com/ (Accessed: 25th August 2022)

Ringraziamenti

Ringrazio innanzitutto la professoressa Elisa Cimetta per avermi dato la possibilità di svolgere la tesi nel suo laboratorio e tutto il team BIAMET per avermi fatto compagnia in questi mesi: Camilla, Caterina, Eleonora, Eva, Federico, Marco e Sara grazie per tutti i momenti passati insieme, per i pranzi sotto i portici o sui gradini (con tanto di mitologia greca by Marco) ed il costante sottofondo musicale in laboratorio. In particolare, grazie alla hit "Gian Marco" scoperta in macchina mentre andavamo in Torre e agli aperitivi sempre molto attesi.

Grazie a Caterina che ha corretto questa tesi e mi ha affiancato in questi mesi: mi hai trasmesso la passione per gli ESOSOMI… ehm no, meglio VESCICOLE EXTRACELLULARI e pazientemente mi hai introdotto al tuo progetto di dottorato. Anche se i chip li facevo sempre troppo spessi, spero di aver contribuito anche solo un minimo al tuo PhD.

Ringrazio i miei amici e colleghi Alessia, Elisa, Ilaria, Luca, Mauro, Serena e Silvia per il reciproco sostegno durante i numerosi progetti, la speranza che Aspen Plus convergesse durante le videochiamate, il disperato tentativo di sdrammatizzare le lezioni e rendere comunque indimenticabile questo bellissimo percorso.

Un sentito ringraziamento ai miei amici delle superiori Alberto, Elena, Giulia e Martina per ormai accompagnarmi da 10 anni. Siamo cresciuti insieme ed è bello vedere come e quanto siamo cambiati in questi anni fortificando la nostra amicizia.

Grazie agli amici di sempre Anna, Annalisa, Claudia, Eli, Giò, Giada, Gian, Nora che fin dall'infanzia sopportano il mio continuo canticchiare, le pazzie, i tanto odiati audio da 10 minuti e le grasse risate tanto da paragonarle a Strega Varana. Mi sa che qualche tarallino e pan cake dopo tutti questi anni ve li siete meritati.

Grazie a Valentina e Benedetta per le sorelle che sono e l'esempio migliore che potessi desiderare; grazie alle mie nipotine Marianna, Alice e Chiara perché anche se non lo sapete, voi mi avete ispirato per questo progetto di tesi.

Grazie anche a me stesso, perché nonostante i diversi ostacoli incontrati, hai avuto il coraggio di rialzarti, riprovare e andare avanti.

Grazie, infine, ai miei genitori per avermi spronato a non mollare quando le cose non andavano come speravo e per avermi dato la possibilità di studiare, senza mettermi pressione. Grazie per l'amore che fin da piccolo mi trasmettete e per averci messo al primo posto nelle vostre scelte: anche se non ve lo dico spesso vi voglio bene!

"La creatività è soprattutto la capacità di porsi continuamente delle domande"

Piero Angela